

## Article

# Spatio-Temporal Evolution of the Crustal Uplift in Eastern NE China: Constraint from Detrital Zircon Ages of Late Mesozoic Clastic Rocks in the Boli Basin

Song He <sup>1,2,3</sup>, Hong Cheng <sup>1,\*</sup>, Shuangqing Li <sup>2,\*</sup>, Cong Cao <sup>3,4</sup>, Jun He <sup>1</sup>  and Fukun Chen <sup>1</sup><sup>1</sup> School of Earth and Space Sciences, University of Science and Technology of China, Hefei 230026, China<sup>2</sup> Institute of Earth Sciences, Heidelberg University, 69120 Heidelberg, Germany<sup>3</sup> Nanjiang Hydrogeological and Engineering Geology Brigade, Chongqing Bureau of Geology and Minerals Exploration, Chongqing 401147, China<sup>4</sup> Laboratory of Chongqing Groundwater Resource Utilization and Environmental Protection, Chongqing 401121, China

\* Correspondence: chsh mily@mail.ustc.edu.cn (H.C.); shuang-qing.li@geow.uni-heidelberg.de (S.L.)

**Abstract:** Detrital zircon of clastic rocks has been widely recognized as a powerful tool for the study of crustal uplift, which is of great significance for understanding multi-sphere interaction. However, young detrital zircons can only roughly constrain the depositional time of the strata, and commonly used zircon age probability density and kernel density estimations cannot provide sufficient evidence to reveal spatio-temporal differences in tectonic uplift. The basins developed in active continental margins usually contain abundant magmatic rocks, which can provide insights into basin evolution and crustal deformation when combined with sedimentary characteristics. In this study, we report detrital zircon ages of Late Mesozoic clastic rocks from the Boli Basin, being part of the Great Sanjiang Basin Group in eastern NE China, which is strongly affected by the Paleo-Pacific subduction. In conjunction with the age data of coeval magmatic rocks and potential sedimentary sources of basement rocks adjacent to the basin, the geochronologic results of this study provide solid evidence for the formation of the Boli Basin and the spatio-temporal evolution of the crustal uplift in northeastern China. The Boli Basin went through multi-phase tectonic evolution of syn-rift and post-rift stages, based on the zircon age data of clastic and igneous rocks. When the geographical distribution characteristics of potential sedimentary sources and their percentages of contribution are taken into account, two stages of eastward migration of the crustal uplift and two episodes of basin destruction caused by the tectonic extension and subsequent compression can be proposed for the Boli Basin. These processes were caused successively by the rolling back of the subducted Paleo-Pacific slab, the docking of the Okhotomorsk block along the eastern continental margin of East Asia, and the transition of the subduction zone by the collision of the Okhotomorsk block.

**Keywords:** Northeast China; Boli Basin; Late Mesozoic; crustal uplift; detrital zircon

**Citation:** He, S.; Cheng, H.; Li, S.; Cao, C.; He, J.; Chen, F. Spatio-Temporal Evolution of the Crustal Uplift in Eastern NE China: Constraint from Detrital Zircon Ages of Late Mesozoic Clastic Rocks in the Boli Basin. *Minerals* **2022**, *12*, 1166. <https://doi.org/10.3390/min12091166>

Academic Editor: Frederick Lin Sutherland

Received: 8 August 2022

Accepted: 9 September 2022

Published: 15 September 2022

**Publisher's Note:** MDPI stays neutral with regard to jurisdictional claims in published maps and institutional affiliations.



**Copyright:** © 2022 by the authors. Licensee MDPI, Basel, Switzerland. This article is an open access article distributed under the terms and conditions of the Creative Commons Attribution (CC BY) license (<https://creativecommons.org/licenses/by/4.0/>).

## 1. Introduction

Basins and ranges are two basic geomorphic units and metallogenic domains of the continent [1–4], the evolution of which has aroused great interest, and is known as “basin-range coupling” [2,5,6]. Differential uplift and subsidence of the crust results in the formation of basins and ranges [7,8]. Thus, studies of crustal uplift contribute to understanding the processes of “basin-range coupling” and related mineral and energy resources. Furthermore, crustal uplift is controlled by crust-mantle geodynamics [9–12] and affects climate by shaping the landscape [13,14]. Hence, research of crustal uplift is of crucial significance for understanding of multi-sphere coupling of the asthenosphere, lithosphere, atmosphere, and biosphere [6,15–18].

Studies of crustal uplift involve various disciplines of geoscience. Paleolatitude variation based on paleomagnetism reveals plateau uplift under the crustal shortening tectonic

settings [19]. The lateral and vertical propagation of magmas provides dynamic evidence for crustal differential uplift [12,20,21]. Moreover, modelling research provides a framework to explain how lithospheric rheology, surface processes, and extensional faults control the height, shape, and longevity of ranges [8,22]. Considering that crustal uplift or exhumation is usually accompanied by cooling processes, the unique closure temperature of different isotopic systems for specific minerals play a crucial role in the process of crustal uplift. Firstly, geochronological and kinematic studies of ductile shear zones in the vicinity of fault belts and metamorphic core complexes can define the timing and mechanism of uplift of the lower-middle crust [23–25]. Secondly, crustal uplift rates can be reconstructed by determining different mineral cooling ages and thermobarometers [26,27]. Moreover, zircon and apatite fission track and (U-Th)/He thermochronology can reveal multi-stage uplift of the orogenic crust [28–30]. Besides, carbonate clumped isotope from carbonates and carbonaceous fossils can recover the paleo-altimetry of the ranges [31,32]. However, studies of geochronology, mineral thermobarometer, and carbonate clumped isotope paleothermometry require ideal objects, which are generally less accessible than clastic rocks from basin-fill. Consequently, revealing crustal uplift based on clastic rocks has been widely used. In the 1980s, provenance and tectonic setting were inferred mainly from detrital framework modes [33] and contents of major, trace, and rare earth elements [34–38]. Radiogenic isotope compositions (e.g., Sr-Nd-Pb) of whole-rocks and single-minerals are also applied to study the provenance and crustal uplift [39–41]. More recently, with advances in in situ analysis, a wealth of research has sprung up and focused on provenance and crustal uplift based on geochronology, trace elemental geochemistry and Hf isotope geochemistry of zircon [42–48].

Many studies have proved the importance of detrital zircon in provenance tracing and crustal uplift [49,50]. However, studies of spatio-temporal differences in crustal uplift using detrital zircon encountered two problems. The youngest detrital zircon (s) have long been applied to infer the maximum depositional age [51], but in practice, it is difficult to precisely limit the actual deposition time of the sedimentary sequence. The geographic distribution of potential provenances (or sedimentary sources) was not considered in the diagrams of zircon age probability density and kernel density estimation [52], making it difficult to reveal differential uplift of the crust. In contrast, basins located on active continental margins are controlled by subduction zones and typically accompanied by coeval volcanic-magmatism. The contact relationships between the volcanic-magmatic rocks and the sedimentary sequences (such as underlying, interbedding, overlying, or intruded) combined with geochronological data of igneous rocks are extremely conducive to constrain stratigraphic ages. In addition, magmatism within the subduction zone is characterized by landward or oceanward migration [53,54], leading to regular change in the spatio-temporal distribution of igneous rocks potentially as sedimentary sources, which can provide a premise for delicate study of differential uplift of the crust.

The Great Sanjiang Basin Group (or “Dasanjiang Basin Group” in the Chinese literature), located in eastern NE China, has experienced a complex tectonic evolution of syn-rift, tectonic inversion, and post-rift processes (Figure 1). The tectonic inversion caused the once-unified basin to split into a series of small ones [55–59]. Due to the disorder of the stratigraphic division, inconsistent dating results by paleontology [60–70] and insufficient U-Pb isotopic ages [71–74], the tectonic frame and history of the basin, even the depositional ages of sedimentary sequences remain to be adequately constrained. In this study, we focus on detrital zircon of Late Mesozoic clastic rocks from the Boli Basin, part of the Great Sanjiang Basin Group. The Late Mesozoic sedimentary sequences fully developed in the Boli Basin, accompanied by coeval magmatism [75–80], which is beneficial for limiting the evolution frame of the basin when combined with the age patterns of detrital zircons in the clastic rocks. The study area was successively influenced by the subduction and closure of the Paleo-Asian Ocean and the Paleo-Pacific Ocean [53,76,81–83], resulting in significant spatio-temporal differences in sedimentary sources and thus, providing a solid basis for the study of differential uplift of the crust. Here, we use line charts of percentage of the source

contribution (detrital zircon age versus potential provenance) to examine the differential uplift of the crust in the Boli Basin and its peripheral.

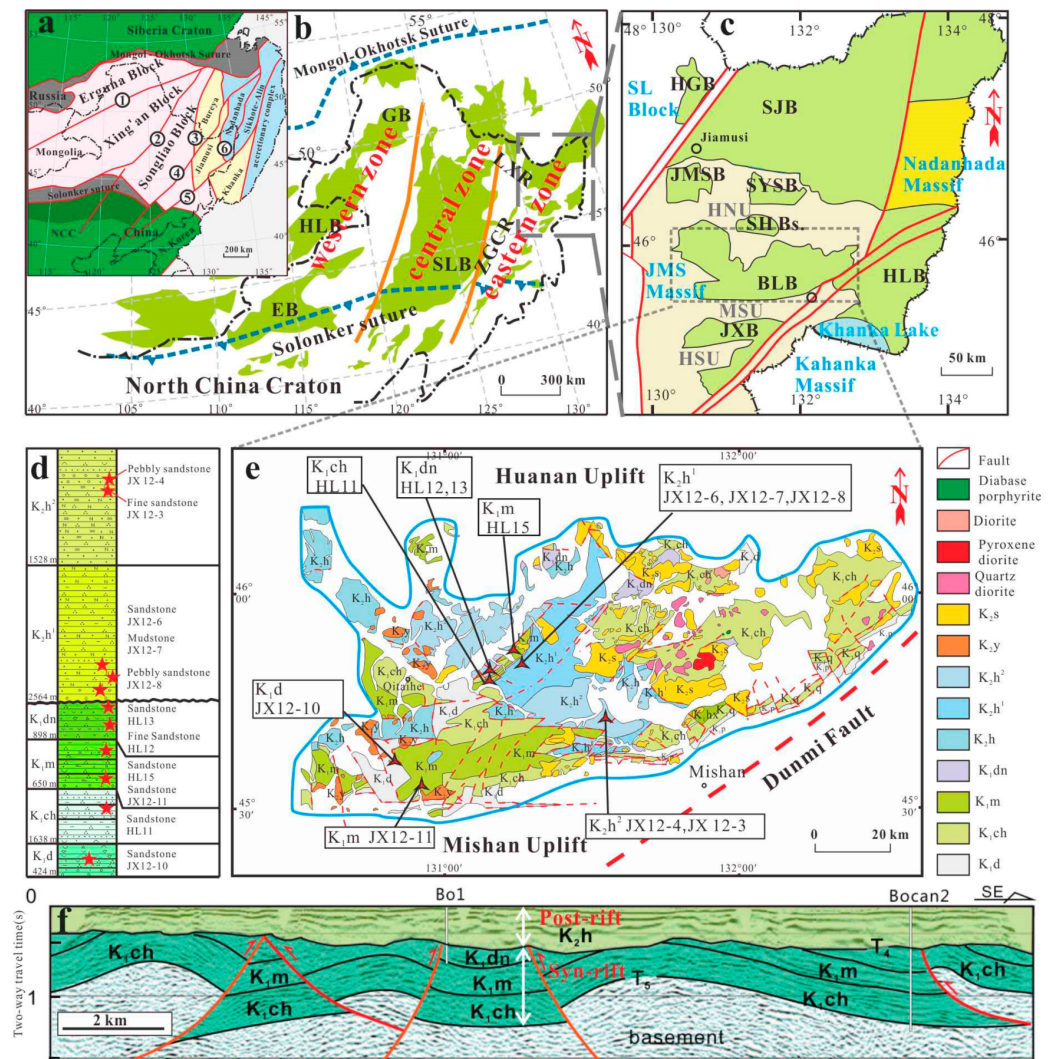


**Figure 1.** Geological map of (a) eastern segment of the Central Asian Orogenic Belt; (b) basin groups in NE China; (c) Great Sanjiang Basin Group; (d,e) stratigraphy and geological map of the Boli Basin, showing distribution of Late Mesozoic clastic rocks and sample localities; (f) seismic profile in the Boli Basin (a,b,f modified after Zhang et al. (2017) [55]). ①: Xinlin-Xiguitu fault; ②: Hegenshan-Heihe fault; ③: Mudanjiang fault; ④: Yilan-Yitong fault; ⑤: Dunhua-Mishan fault; ⑥: Yuejinshan fault; EB-Erlian Basin, GB-Genhe Basin, SLB-Songliao Basin, HGB-Hegang Basin, SJB-Sanjiang Basin, JMSB-Jiamusi Basin, SYSB-Shuangyashan Basin, SHB-Shuanghua Basin, BLB-Boli Basin, JXB-Jixi Basin, HLB-Hulin Basin; HNU-Huanan uplift, MSU-Mishan uplift, HSU-Hengshan uplift, LXR-Lesser Xing’an Range, ZGCR-Zhuangguangcai Range.

**2. Geological Background and Samples**

The Boli Basin in Northeast China is located in the zone among the Siberian Block, North China Block, and West Pacific Plate, and is part of the eastern segment of the Central Asian Orogenic Belt (Figure 1a). Northeast China geologically consists of the Erguna, Xing’an, Songliao, and Bureya-Jiamusi-Khanka massifs (known as the “Northeast Micro-block Group” in the Chinese literature), and part of the North China Block in the south and the Wanda Range (or Nadanhada) and Sikhote-Alin accretionary complex in the east. The above-mentioned blocks or massifs are separated by the Mongolia-Okhotsk suture zone and the Solonker suture zone (Figure 1b). As a result, NE China was influenced by

the tectonic domains of the Paleo-Asian Ocean, the Mongolian-Okhotsk Ocean, and the Paleo-Pacific Ocean, and hence, underwent a complex tectonic evolution, accompanied by extensive volcanic-magmatic activity [75,84,85]. The landform in NE China shows a basin-range configuration that can be divided into western, central, and eastern basin groups (Figure 1b) [55]. It is noteworthy that the eastern basin group, termed as the Great Sanjiang Basin Group (GSJBG), underwent more dramatic compression in the middle Cretaceous, resulting in the formation of a series of isolated small basins (Figure 1c) [55–59].

The Boli Basin is located in the southern part of the Great Sanjiang Basin Group and developed on the Jiamusi Massif (Figure 1c). It is separated from the Jixi Basin by the Mishan Uplift in the south, from the Sanjiang Basin by the Huanan Uplift in the north, and from the Hulin Basin by the Dun-Mi Fault in the east (Figure 1c). This basin was mainly filled with Late Mesozoic clastic rocks with subordinate tephra interlayers. The Jixi Group developed during the syn-rift period (Early Cretaceous), including the Didao Formation ( $K_1d$ ), Chengzihe Formation ( $K_1ch$ ), Muling Formation ( $K_1m$ ), and Dongshan Formation ( $K_1dn$ ) from bottom to top. The Houshigou Formation ( $K_2h$ ) developed during the post-rift period (Late Cretaceous) and can be divided into the lower and upper sections (Figure 1d–f). The coeval volcanic rocks were developed in the Boli Basin, termed the Songmuhe Formation in the east and Yilin Formation in the west, mainly consisting of rhyolite, dacite, and andesitic porphyrite. In addition, sporadic magmatic rocks, mainly consisting of rhyolite and diabase porphyrite, intruded into the syn-rift strata (Figure 1e).

Ten samples of clastic rocks were collected from the sedimentary sequences in the Boli Basin for zircon U-Pb dating, including (1) sandstone from the Didao and Muling formations ( $K_1d$ , sample JX12-10;  $K_1m$ , sample JX12-11) in the southwestern part of the basin (Figures 1d,e and 2a,b); (2) sandstone from the Chengzihe, Muling, and Dongshan formations ( $K_1ch$ , sample HL11;  $K_1m$ , sample HL15;  $K_1dn$ , samples HL12 and HL13) in the central basin (Figures 1d,e and 2c,d); and (3) sandstone and pebbly sandstone from the lower section of the Houshigou Formation ( $K_2h^1$ , samples JX12-6 and JX12-8), siltstone (sample JX12-3) and pebbly sandstone (sample JX12-4) from the upper section of the formation ( $K_2h^2$ ) in the east-central basin (Figures 1d,e and 2e,f).



**Figure 2.** Photographs of outcrops and micro-photos of Late Mesozoic clastic rocks of the Boli Basin: (a,b) sandstone from the Muling and Didao formations ( $K_1m$ , JX12-11;  $K_1d$ , JX12-10) in the southwestern basin; (c,d) sandstone with fossil from the Muling and Chengzihe formations ( $K_1m$ , HL15;  $K_1ch$ , HL11) in the middle basin; (e,f) pebbly sandstone and mudstone ( $K_2h$ , JX12-7, -8, -4) from the Houshigou Formation. Abbreviation: Q-quartz; Pl-plagioclase; Bi-biotite.

### 3. Analytical Methods and Analytical Results

Approximately 2 kg of each sample was crushed for zircon separation using standard mineral separation techniques. Zircon crystals were handpicked under a microscope,

mounted in epoxy, and then polished for analysis. Cathodoluminescence (CL) images of zircon grains were obtained to inspect their internal structures for in situ U-Pb isotopic analysis. A laser ablation-inductively coupled plasma-mass spectrometer (LA-ICP-MS) located in the Key Laboratory of Crust-Mantle Materials and Environments, University of Science and Technology of China, was employed for zircon U-Pb dating. Zircon 91500 was used as an external standard for calibration of U-Pb and was analyzed twice per ten analyses. Procedures are described in detail elsewhere [86]. Correction for common Pb was performed using the ComPbCorr#3\_18 procedure [87], U-Pb isotopic ratios were calculated using the ICPMSDataCal software module [86], and U-Pb age calculations were performed using ISOPLOT 4.15 [88]. All uncertainties for individual analyses are quoted as 1 $\sigma$ .

Analytical results of the U-Pb dating on detrital zircon grains separated from Late Mesozoic clastic rocks of the Boli Basin are given as Supplementary Data in Table S1. Plots of U-Pb isotopic data and diagram of Th/U ratio versus age of zircons are shown in Figure 3, while diagrams of probability density and representative CL images of detrital zircon are shown in Figure 4. In this study, analytical spots with a concordance greater than 90% are selected for the data evaluation.  $^{206}\text{Pb}/^{238}\text{U}$  ages are used for grains younger than 1.0 Ga and  $^{207}\text{Pb}/^{206}\text{Pb}$  ages for those older than 1.0 Ga.

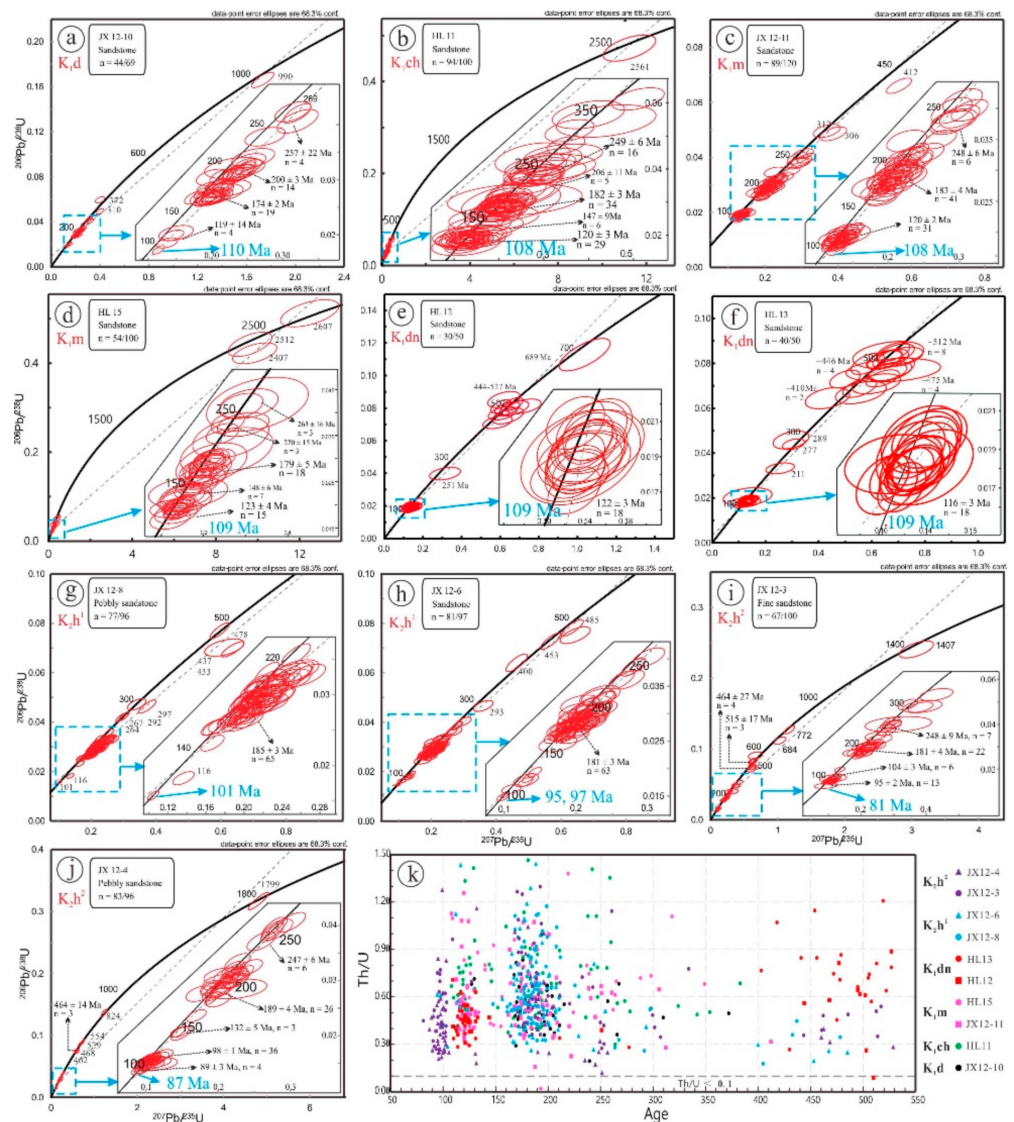


Figure 3. Zircon U-Pb concordia diagrams of Late Mesozoic clastic rocks from the Boli Basin.

Detrital zircon grains from the southwestern Boli Basin (Figure 4a,c) are euhedral to subhedral crystal and angular to subangular, with larger sizes than those from the central basin (Figure 4b,d–f), implying shorter to moderate transport before deposition. Detrital zircon grains from the central basin are of two types, younger ones (133–109 Ma) are euhedral to subhedral crystal and are angular to subangular (Figure 4b,d–h), reflecting shorter transport from adjacent areas, while the older ones (>131 Ma) are subhedral to anhedral crystal and subcircular to subangular, reflecting longer transport distances from distant provenances. Detrital zircon grains from the eastern basin are subangular to subrounded (Figure 4i,j), indicating a long transport distance. Almost all the zircon grains have Th/U ratios of 0.12 to 2.62 (Figure 3k) and mostly have oscillatory cathodoluminescence zone, suggesting magmatic origin.

**Didao Formation (K<sub>1</sub>d):** A total of sixty-nine detrital zircon grains from the sandstone sample JX12-10 were selected for the U-Pb dating. Forty-four analytical spots having concordant U-Pb ages yield a broad age range from ~990 Ma to ~110 Ma. They define four main populations with <sup>206</sup>Pb/<sup>238</sup>U ages of 119 ± 14 Ma (n = 4), 174 ± 2 Ma (n = 19), 200 ± 3 Ma (n = 14), and 257 ± 22 Ma (n = 4), respectively. The other three grains crystallized in the Late Permian (310 Ma), Late Devonian (372 Ma), and Neoproterozoic (990 Ma), respectively (Figure 3a). Two major age peaks at ~174 Ma and ~200 Ma are shown in the diagram of probability density (Figure 4a).

**Chengzihe Formation (K<sub>1</sub>ch):** Ninety-four out of one hundred zircon grains from the sandstone sample HL11 yield concordant U-Pb ages. Their <sup>206</sup>Pb/<sup>238</sup>U age values vary from 383 Ma to 108 Ma, with one exceptional grain with a <sup>207</sup>Pb/<sup>206</sup>Pb age of 2561 Ma. The three main age populations can be recognized with a weighted mean <sup>206</sup>Pb/<sup>238</sup>U ages of 120 ± 3 Ma (n = 29), 182 ± 3 Ma (n = 34) and 249 ± 6 Ma (n = 16), respectively. In addition, two minor age groups with mean <sup>206</sup>Pb/<sup>238</sup>U ages of 147 ± 9 Ma (n = 6) and 206 ± 11 Ma (n = 5) can be identified (Figures 3b and 4b). Five single grains give ages of Early Permian (298 Ma), Early Carboniferous (324, 342, 354 Ma), and Devonian (383 Ma).

**Muling Formation (K<sub>1</sub>m):** Eighty-seven out of one hundred and twenty analyzed zircon grains from the sample JX12-11 in the southwestern Boli Basin yield concordant U-Pb ages, ranging from 412 Ma to 108 Ma. The age data can be subdivided into three major populations with weighted mean <sup>206</sup>Pb/<sup>238</sup>U ages of 120 ± 2 Ma (n = 31), 183 ± 4 Ma (n = 41), and 248 ± 6 Ma (n = 6), respectively (Figure 3c). Other grains give Late Carboniferous and Early Devonian ages (Figure 4c). Fifty-four out of one hundred zircon grains from sample HL15 in the central Boli Basin were plotted on the U-Pb concordia curve. Three grains yield Paleo-Proterozoic and Archean <sup>207</sup>Pb/<sup>206</sup>Pb ages (2407 Ma, 2512 Ma, and 2607 Ma) and the remaining zircon grains have young <sup>206</sup>Pb/<sup>238</sup>U ages from 348 Ma to 109 Ma. These young zircon grains can be divided into two major age populations of 123 ± 4 Ma (n = 15) and 179 ± 5 Ma (n = 18) and three minor age populations of 148 ± 6 Ma (n = 7), 220 ± 15 Ma (n = 3), and 263 ± 16 Ma (n = 3), respectively (Figure 3d). In the probability density diagram (Figure 4d), the age peaks of 179 Ma and 123 Ma are obvious, and some zircon grains have ages of Early Permian (298–288 Ma) and Early Carboniferous (349–318 Ma).

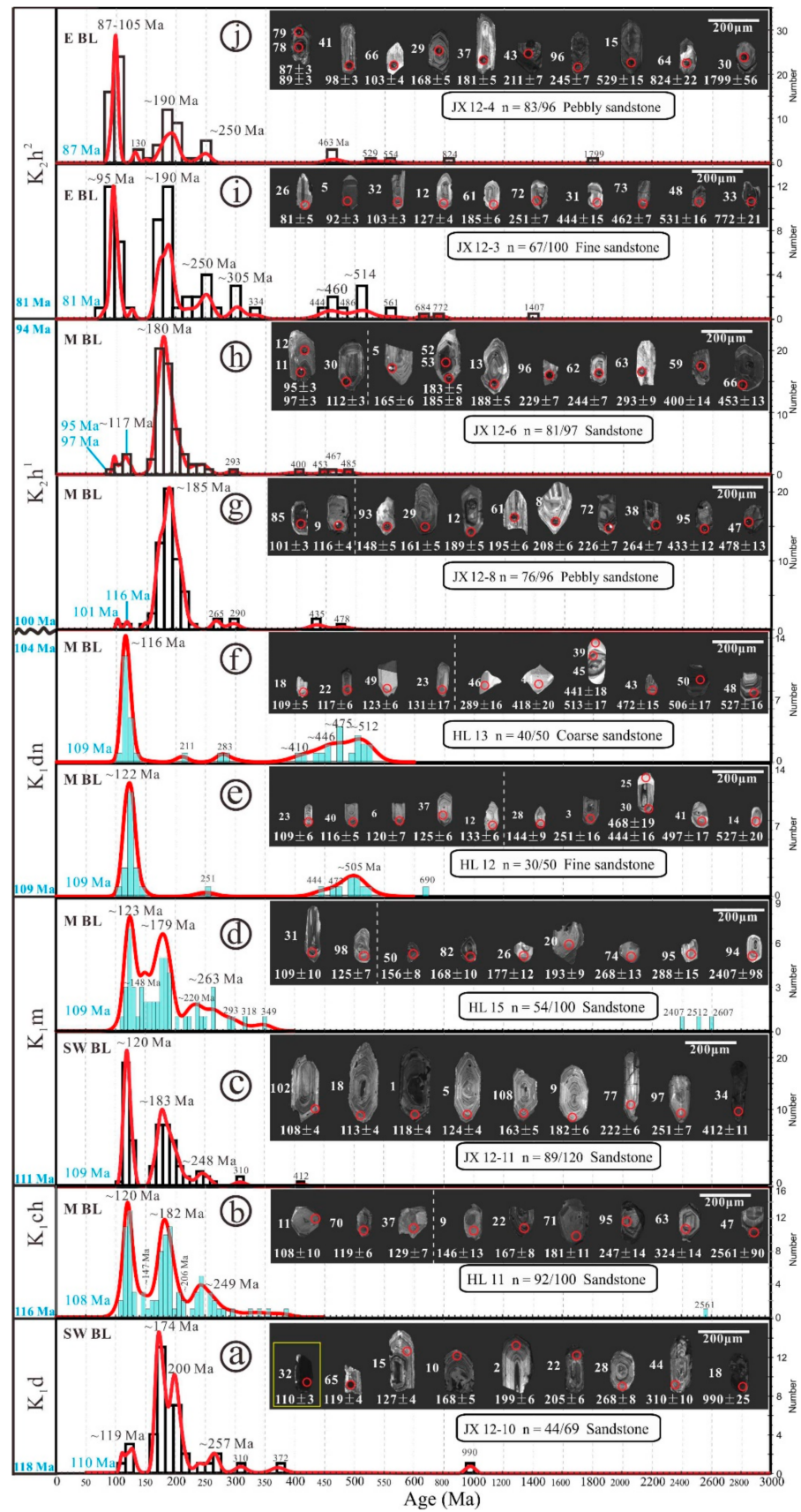


Figure 4. Zircon CL images and U-Pb probability density diagrams of clastic rocks from the Boli Basin.

**Dongshan Formation (K<sub>1</sub>dn):** Fifty zircon grains from the sandstone sample HL12 in the central Boli Basin were analyzed, and thirty analytical spots yield concordant U-Pb ages. These zircon grains cluster at two major age peaks of  $122 \pm 3$  Ma ( $^{206}\text{Pb}/^{238}\text{U}$ ,  $n = 18$ ) and  $505 \pm 14$  Ma ( $^{206}\text{Pb}/^{238}\text{U}$ ,  $n = 14$ ) (Figure 3e). In addition, single zircon ages of 144 Ma, 251 Ma, 444 Ma, 468 Ma, 477 Ma, and 689 Ma were also found (Figure 4e). The sandstone sample HL13 has a similar distribution of detrital zircon ages to sample HL12. Fifty zircon grains were analyzed, and forty-one analytical spots have concordant U-Pb ages, where all of them were younger than 527 Ma. The most significant age group is clustered at 131 Ma to 109 Ma, giving an age peak at 116 Ma ( $n = 18$ ). Three subordinate age peaks can be seen at 446 Ma ( $n = 4$ ), 475 Ma ( $n = 4$ ), and 512 Ma ( $n = 8$ ) (Figure 3f). The remaining zircon grains yield  $^{206}\text{Pb}/^{238}\text{U}$  ages of 211 Ma, 277 Ma, 289 Ma, 403 Ma, and 418 Ma (Figure 4f).

**Lower section of the Houshigou Formation (K<sub>2</sub>h<sup>1</sup>):** Seventy-six out of ninety-six grains from the pebbly sandstone sample JX12-8 yield concordant U-Pb ages, exhibiting a board range from 478 Ma to 101 Ma. One pronounced age population gives a weighted mean  $^{206}\text{Pb}/^{238}\text{U}$  age of  $185 \pm 3$  Ma ( $n = 65$ ) (Figure 3g). The Early Cretaceous zircons (116 Ma to 101 Ma) contained in this sample became less significant compared with the clastic rocks of the Chengzihe (K<sub>1</sub>ch) and Dongshan (K<sub>1</sub>dn) formations. Minor zircon grains of Permian (297–264 Ma) and Early Paleozoic (478–435 Ma) can be also found (Figure 4g). The sandstone sample JX12-6 from the same locality has a similar distribution of zircon ages to sample JX12-8. Analyses of the U-Pb isotopic dating were performed on a total of ninety-seven zircon grains and eighty-one analytical spots yield concordant U-Pb ages, ranging from 485 Ma to 95 Ma. The majority of the age values give a weighted mean  $^{206}\text{Pb}/^{238}\text{U}$  age of  $181 \pm 3$  Ma ( $n = 63$ ) (Figure 3h). Minor age groups are Cretaceous (124–95 Ma), Early Permian (293 Ma), Early Devonian (400 Ma), and Ordovician (485–453 Ma), respectively (Figure 4h).

**Upper section of the Houshigou Formation (K<sub>2</sub>h<sup>2</sup>):** Analyses of one hundred zircon grains were performed for the fine sandstone sample JX12-3 from the eastern Boli Basin, where sixty-seven analytical spots yield concordant U-Pb ages, ranging from 1407 Ma to 81 Ma. Six major age populations with weighted mean ages of  $95 \pm 2$  Ma ( $n = 13$ ),  $104 \pm 3$  Ma ( $n = 6$ ),  $181 \pm 4$  Ma ( $n = 22$ ),  $248 \pm 9$  Ma ( $n = 7$ ),  $464 \pm 27$  Ma ( $n = 4$ ), and  $515 \pm 17$  Ma ( $n = 3$ ) can be obtained (Figure 3i). The remaining grain formed in the Carboniferous (334–300 Ma), Neoproterozoic (772–561 Ma) and Mesoproterozoic (1407 Ma) (Figure 4i). The pebbly sandstone sample JX12-4 has a similar age distribution to sample JX12-3. Eighty-three analytical spots out of ninety-six detrital zircon grains yield concordant U-Pb ages, defining a broad age range from 1799 Ma to 87 Ma. Six major age populations can be identified (Figure 3j), having weighted mean  $^{206}\text{Pb}/^{238}\text{U}$  ages of  $89 \pm 3$  Ma ( $n = 4$ ),  $98 \pm 1$  Ma ( $n = 36$ ),  $132 \pm 5$  Ma ( $n = 3$ ),  $189 \pm 4$  Ma ( $n = 26$ ),  $247 \pm 6$  Ma ( $n = 6$ ), and  $464 \pm 14$  Ma ( $n = 3$ ), respectively. The other analytical spots give U-Pb ages of Cambrian (529 Ma), Neoproterozoic (824–554 Ma), and Paleoproterozoic (1799 Ma) (Figure 4j).

#### 4. Potential Sedimentary Sources Adjacent to the Boli Basin

Phanerozoic magmatic rocks were well developed on the Great Sanjiang Basin Group and adjacent areas, defining potential provenance for the basin filling. Based on the compilation of a large data set for more than 500 samples, including age and geographical data (Figures 5 and 6), comprehensive information of the provenances can be acquired and in favor of reconstructing provenance variation and differential uplift of the crust during the formation of the Boli Basin. On the basis of the data set, we can distinguish four major regions of potential provenances to provide sedimentary material: western provenances (W-x), middle provenances (M-x), eastern provenances (E-x), and coeval volcanic-magmatic provenances (VM-x), where x means from 1 to 5, representing the number of sub-provenances.

**Western potential provenances (W-x):** Potential sources of W-1 to W-5 are distributed in the Zhangguangcai Range on the western part of the Great Sanjiang Basin Group (Figures 5 and 6). Rocks of W-1 (190–170 Ma) were found in the westernmost part of

the Zhangguangcai Range, adjacent to the Songliao Basin, thus being the westernmost potential source for the basin filling of the Great Sanjiang Basin Group [75,78,81,84,89–99]. Source rocks of W-2 (205–190 Ma) are located in the central region of the Zhangguangcai Range [81,82,84,89,90,92–94,100–104] and rocks of W-3 (370–310 Ma) are in the southern part of the range (between W-2 and W-4) [84,105,106]. Rocks of W-4 (235–205 Ma) are mainly located in the western part of the Mudanjiang fault and subordinately from the Jiamusi Massif [75,81,82,84,93,94,100,101,103,104,107–113], while those of W-5 (490–410 Ma) are distributed mainly in the western part of the Mudanjiang fault and subordinately from the northeastern Boli Basin [114–118] (Figure 5).

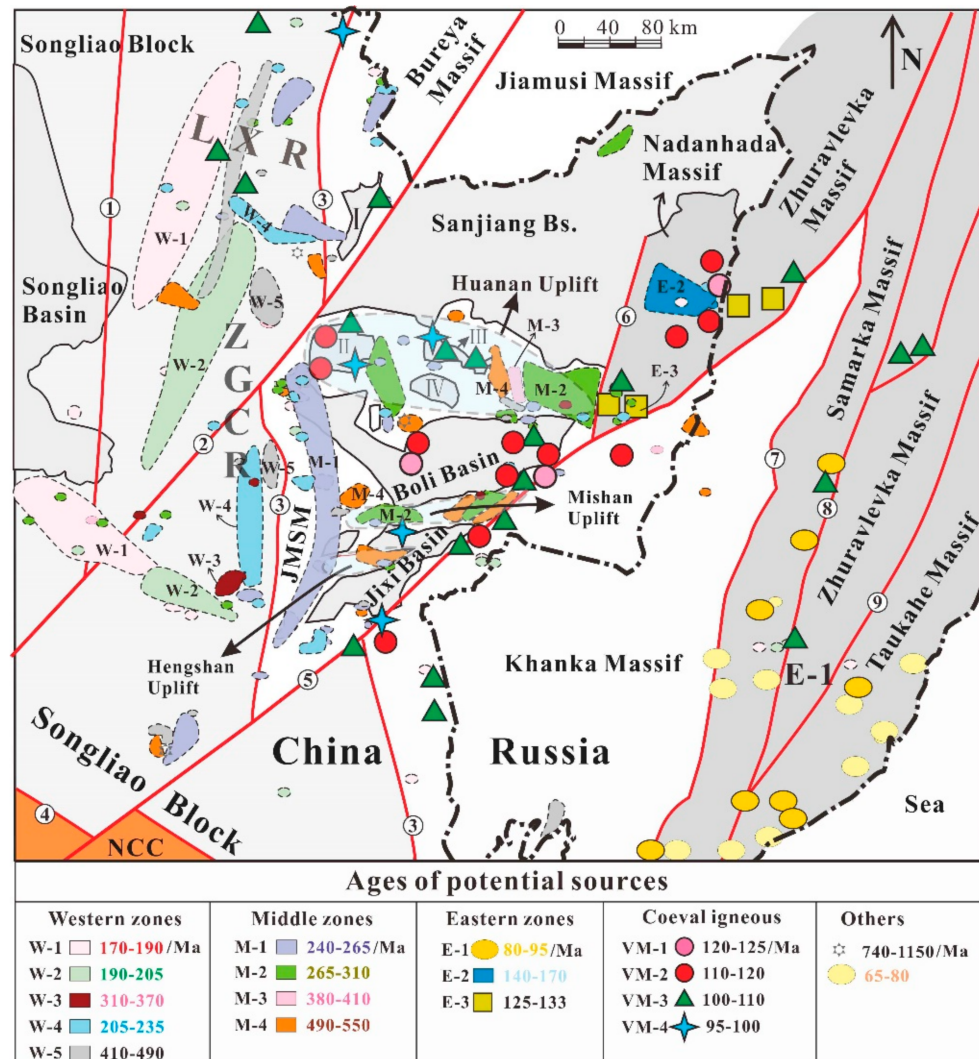


**Figure 5.** Geological map showing distribution map of the potential provenances for the basin filling. I-Hegang Basin, II-Jiamusi Basin, III-Shuangyashan Basin, IV-Shuanghua Basin; ①: Xunke-tieli-shangzhi fault, ②: Jiayi fault, ③: Mudanjiang fault, ④: Xilamulunhe suture, ⑤: Dunmi fault, ⑥: Yuejinshan fault, ⑦: Arsen’evsky fault, ⑧: Central Sikhote-Alin fault, ⑨: Fourmanovsky fault; LXR-Lesser Xing’an Range, ZGCR-Zhangguangcai Range, JMSM-Jiamusi massif.

**Middle potential provenances (M-x):** The middle potential provenances are located in the Jiamusi Massif and are composed of Cambrian to Triassic rocks (Figures 5 and 6). Source M-1 (265–240 Ma) is mainly developed in the western Jiamusi Massif and subordinately along the western part of the Mudanjiang fault [81,90,93,94,104,108,110,119–129]. Source M-2 (310–265 Ma) is mostly located in the Mishan and Huanan uplifts within the Jiamusi Massif with a small amount in the Zhangguangcai Range [82,90,108,120,123,126,127,130–138]. Source

M-3 (410–380 Ma) develops mainly in the eastern part of the Huanan Uplift and subordinately in the western of Jiamusi Basin [96,139,140]. Source M-4 (550–490 Ma) is found mainly in the Hengshan, Mishan, and Huanan uplifts within the Jiamusi Massif and subordinately in the northern Zhangguangcai Range and the eastern Khanka Massif [83,117,118,141–145].

**Eastern potential provenances (E-x):** Three potential source areas can be recognized in the eastern region of the Boli Basin, which is mainly composed of a series of accretionary complexes, including the Nadanhada, Samarka, Zhuravlevka, and Taukahe massifs (Figures 5 and 6). Source E-1 (95–80 Ma) is distributed in the Samarka, Zhuravlevka, and Taukahe massifs that are located in Russia’s Primorsky Krai [146–149]. Source E-2 (170–140 Ma) was only found in the northern part of the Nadanhada Massif [150–153]. Source E-3 (140–125 Ma) was found in Dongfanghong and Raohe, close to the northeastern margin of the Boli Basin [75,147,152,154,155].

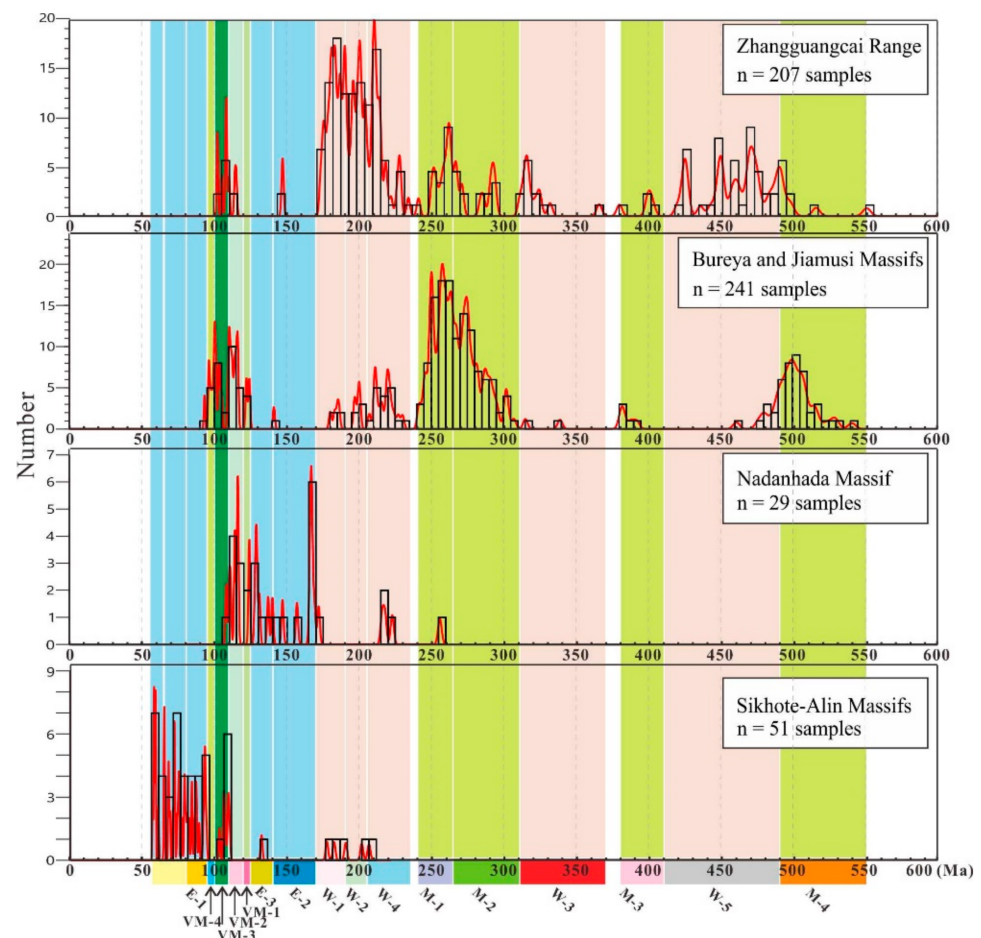


**Figure 6.** Probability density diagrams of potential provenances for sedimentary strata of the Boli Basin.

**Coeval volcanic-magmatic potential provenances (VM-x):** The formation of the Great Sanjiang Basin Group was accompanied by coeval volcano-magmatism, mainly distributed within the basins and in the Lesser Xing’an Range in the northwest and the accretionary complex belt in the east (Figures 5 and 6). Rocks of VM-1 (125–120 Ma) are mainly developed in the middle-east part of the Boli Basin and the northern part of the Nadanhada Massif [75,153,156]. Rocks of VM-2 (120–110 Ma) are mainly found in the Boli, Jiamusi, and Hulin basins and the Nadanhada Massif [75,153,156–158]. Rocks of VM-3 (110–100 Ma) spread over the Great Sanjiang Basin Group and its periphery [75,78,146,147,149,156,159] and rocks of VM-4 (100–95 Ma) can be found in the Jixi, Jiamusi, and Shuangyashan basins [75–77,79,156].

### 5. Discussion

#### 5.1. Constraints on Depositional Time of the Sedimentary Sequences

It is well known that the sedimentary ages of clastic rocks are difficult to obtain, unless volcanic layers can be found interbedded in the sedimentary sequences. Such igneous products are most conducive to constraining the depositional time of sedimentary rocks. For clastic rocks without tephra interlayers, the maximum depositional age is generally inferred by the youngest detrital zircons or the ages of the underlying geological bodies, while the minimum depositional age can be constrained by the overlying sequence or igneous rocks intruding into the clastic strata. Considering that the Great Sanjiang Basin Group was once a unified basin during the syn-rift period [55–59], in this study, we tentatively assume that the analyzed samples of the same rock sequences or formations, although presently located in isolated sub-basins due to late tectonic events, should share a unified depositional time. To reduce the influence of the age errors of the youngest detrital zircons on the depositional ages, we integrate age data of the youngest detrital zircons, tephra interlayers, volcanic layers, underlying and overlying sequences, and igneous rocks intruding into the clastic rocks in the Great Sanjiang Basin Group. Collective constraints on depositional age and relevant data on the sedimentary sequences or formations in different basins of eastern NE China are summarized in Figure 7.

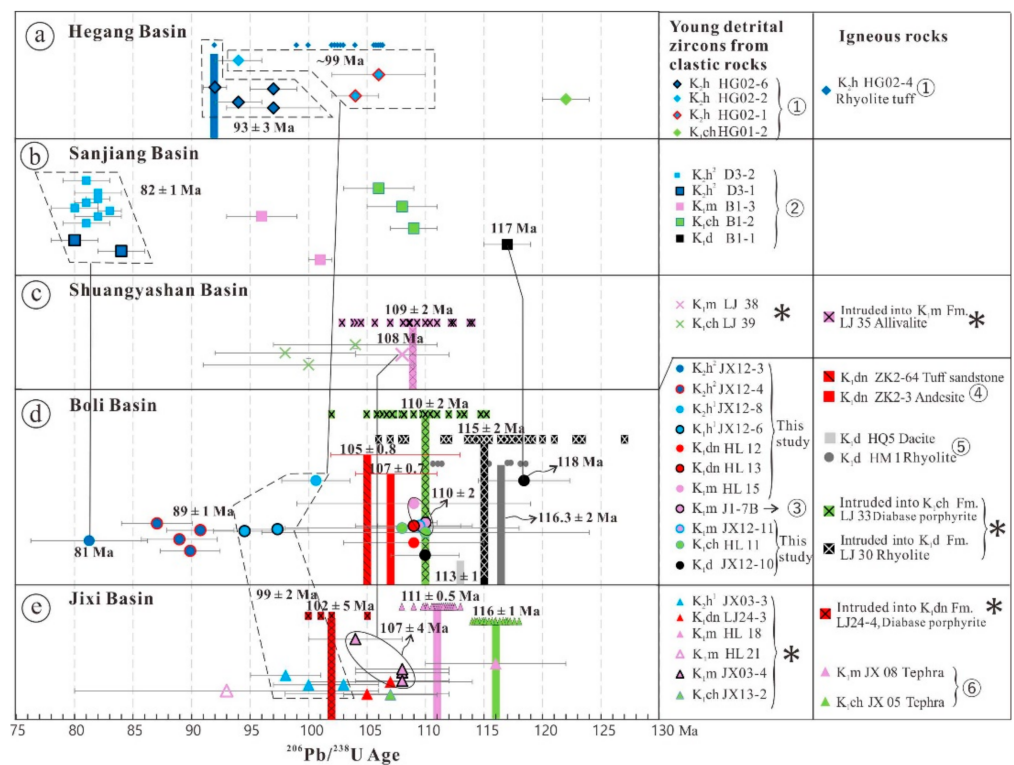


**Figure 7.** Time frame of the Great Sanjiang Basin Group, constrained by the dating results of clastic and magmatic rocks. (a–e) time frame of Hegang, Sanjiang, Shuangyashan, Boli and Jixi basins, respectively. ①: clastic rocks from the Hegang Basin [71]; ②: clastic rocks from the Sanjiang Basin [72]; ③: clastic rocks of the Muling Formation ( $K_1m$ ) from the Jixi Basin [160]; ④: tuff sandstone and andesite of the Dongshan Formation ( $K_1dn$ ) from the Boli Basin [74]; ⑤: dacite and rhyolite of the Didao Formation ( $K_1d$ ) and Peide Formation from the Boli Basin [156]; ⑥: tephra of the Chengzihe ( $K_1ch$ ) and Muling ( $K_1m$ ) formations from the Jixi Basin [73]; \*: authors’ unpublished data.

**Didao Formation ( $K_1d$ ):** An age of  $110 \pm 2$  Ma was obtained from the youngest detrital zircon grain of sandstone sample JX12-10 (Figure 7d). However, this grain has very high U content (~2170 ppm, Table S1) and uniformly dark CL image (Figure 4a), likely implying late hydrothermal or metamict overprint that can lead the loss of radiogenic Pb,

consequently showing a younger age (Figure 3a). Apart from this zircon grain, another zircon grain has relatively low U and Th contents (679 and 332 ppm) and gives an age value of 118 Ma. This is consistent with the depositional age of  $117 \pm 2$  Ma for the Didao Formation in the Sanjiang basin, constrained by the youngest detrital zircon U-Pb age (Figure 7b) [72]. Furthermore, an emplacement age of  $116.3 \pm 2.1$  Ma was reported for rhyolite within the Peide Formation (equivalent to the Didao Formation) in the eastern Boli Basin (Figure 7d) [156], consistent with the ages of the youngest detrital zircons. A zircon age of  $116 \pm 1$  Ma was reported for tephra interlayer collected from the overlying Chengzihe Formation in the Jixi Basin (Figure 7e) [73], which can place a limit of the minimum depositional age of the Didao Formation. Similarly, an eruptive age of  $115 \pm 2$  Ma was obtained for rhyolite overlaying the Didao Formation (authors' unpublished data). Therefore, we can infer that the sedimentary sequences of the Didao Formation were more likely deposited between 118 Ma and 116 Ma (Figure 7).

**Chengzihe Formation (K<sub>1</sub>ch):** Sandstone of the Chengzihe Formation collected from the Jixi, Boli, and Shuangyashan basins contain the youngest detrital zircon grains of 107 Ma (Figure 7e, JX13-2), 110–108 Ma (Figure 7d, HL11), and 104–98 Ma (Figure 7c, LJ39), respectively. Previous studies also reported youngest detrital zircon ages of 109–106 Ma (Figure 7b, B1-2) and 122 Ma (Figure 7a, HG1-02) for the Chengzihe Formation in the Sanjiang and Hegang basins [71,72]. Conclusively, the depositional time of this formation likely ranged from 122 Ma to 98 Ma. However, diabase porphyrite intruding the Chengzihe Formation in the Boli Basin was emplaced at  $110 \pm 2$  Ma (Figure 7d, LJ33, authors' unpublished data), indicating that the depositional age should be older than 110 Ma. Moreover, an age of  $111.1 \pm 0.5$  Ma (Figure 7e, JX08) was reported for tephra interlayer collected from the boundary of the Chengzihe and Muling formations [73]. In summary, timing of deposition of the Chengzihe Formation in the Great Sanjiang Basin Group cannot be constrained solely by the youngest detrital zircons from clastic rocks, due to its wide range of U-Pb age values. Here, we propose a depositional age of 116 Ma to 111 Ma for the Chengzihe Formation in combination of the minimum depositional age of the Didao Formation and the emplacement ages of tephra and magmatic rocks.

**Muling Formation (K<sub>1</sub>m):** Synthesizing the results of this study and previously reported age data [72,160], the youngest detrital zircon ages of the Muling Formation in the Great Sanjiang Basin Group range from 116 Ma to 93 Ma. The dominant ages are  $110 \pm 2$  Ma (Figure 7d, JX12-11, J1-7B, HL15) and  $107 \pm 4$  Ma (Figure 7e, JX03-4), while the minor ages are  $116 \pm 6$  Ma (Figure 7e, HL18),  $101 \pm 1$  Ma and  $96 \pm 3$  Ma (Figure 7b, B1-3) [72], and  $93 \pm 13$  Ma (Figure 7e, HL21). However, the boundary of the Chengzihe and Muling formations was placed at around 111 Ma [73] (Figure 7e, JX08). The pluton intruding the Muling Formation was emplaced at  $109 \pm 2$  Ma (Figure 7c, LJ35). Hence, the depositional age of the Muling Formation can be constrained at 111 Ma to 109 Ma, which is in agreement with the ages of the youngest detrital zircon grains of 110 Ma to 107 Ma.

**Dongshan Formation (K<sub>1</sub>dn):** The U-Pb ages of the youngest detrital zircon grains from the Dongshan Formation in the Jixi and Boli basins range from 109 Ma to 105 Ma, likely being the depositional age of this formation (Figure 7d,e, HL12-13, LJ24-3). Considering the conformable contact of the Dongshan Formation and underlying Muling Formation (Figure 1f), the age value of 109 Ma should be the maximum depositional age of the Dongshan Formation and the minimum age of the Muling Formation. Andesite of  $107.2 \pm 0.7$  Ma at the bottom and tuffaceous sandstone of  $105.0 \pm 0.8$  Ma at the top of the Dongshan Formation collected from a drilling hole have suggested that this formation should develop at least from 107 Ma to 105 Ma (Figure 7d, ZK2-3, -64) [74]. In addition, gabbro intruding into the Dongshan Formation was emplaced at 102 Ma (Figure 7e, LJ24-4), suggesting that the sedimentation ended before 102 Ma. Furthermore, in combination with the tectonic inversion after the Dongshan Formation [55] and the sudden cessation of magmatic activities in the Great Sanjiang Basin Group and its periphery after ~104 Ma (authors' unpublished data), we suggest 104 Ma as the minimum depositional age of the Dongshan Formation.

**Houshigou Formation (K<sub>2</sub>h):** Clastic rocks of the lower sequence of the Houshigou Formation in the Jixi and Boli basins contain the youngest detrital zircon grains of 103 Ma to 95 Ma (Figure 7d,e, JX03-3, 12-6, 12-8), which is consistent with those of 104 Ma to 94 Ma in the Hegang Basin (Figure 7a, HG02-1, -2) [71]. They yield a weighted mean age of ~100 Ma, which is suggested as the maximum depositional age for the lower sequence. Age data of tuffs and sandstones from the Hegang Basin indicate that the upper sequence of the Houshigou Formation was deposited at ~93 Ma (Figure 7a) [71]. Sandstones of the equal sequence collected from the Boli Basin contain the youngest detrital zircon grains of ~81 Ma (Figure 7d, JX12-3), similar to the age of 82 ± 1 Ma reported for clastic rocks in the Sanjiang Basin (Figure 7b, D3-1, -2) [72], which indicates the deposition of the upper sequence should be lasted until at least ~81 Ma.

### 5.2. Spatio-Temporal Evolution of the Crustal Uplift

Due to the complexity of potential provenances, it is difficult to identify the spatio-temporal differences in the crustal uplift in detail solely by comparing probability densities between the samples in the basin and the potential provenances (Figures 4 and 6). To analyze the contributions made by different provenances, percentages of the source contributions to the basin filling from different provenances for each sample were calculated (see Table 1) and line charts of the percentages are shown in Figure 8. The horizontal axis is designated, from left to right, to the western, middle, coeval igneous, and eastern potential provenances, while the vertical axis indicates the percentages of source contribution. As shown in Figure 8a, the black line indicates the percentages of contributions made by each potential provenance to sandstone sample JX12-10 from the Didao Formation, visually revealing that the western zone (or the Zhangguangcai Range) provides a significant contribution; among them, the contribution from W-1 is the highest, reaching up to ~36% (Figure 8a and Table 1). Compared to the diagrams of zircon probability density and kernel density estimation, line charts of percentages of source contribution explicitly reveal the spatio-temporal differences in the process of the crustal uplift. By means of the line charts used here, we can propose that the crust of the Boli Basin and its periphery experienced four stages of the uplift, i.e., eastward migration of the crustal uplift, uplift of basement of the Jiamusi Massif, western crustal uplift, and formation of the eastern Coastal Ranges (Figure 8). Sketch models for the processes of the crustal uplift and corresponding tectonic evolution are shown in Figure 9.

**Table 1.** Contribution percentage (%) of potential sources for the samples in the Boli basin.

| Sample     | JX12-10          | JX12-11          | HL11              | HL15             | HL12              | HL13              | JX12-8                        | JX12-6                        | JX12-3                        | JX12-4                        |
|------------|------------------|------------------|-------------------|------------------|-------------------|-------------------|-------------------------------|-------------------------------|-------------------------------|-------------------------------|
| Source No. | K <sub>1</sub> d | K <sub>1</sub> m | K <sub>1</sub> ch | K <sub>1</sub> m | K <sub>1</sub> dn | K <sub>1</sub> dn | K <sub>2</sub> h <sup>1</sup> | K <sub>2</sub> h <sup>1</sup> | K <sub>2</sub> h <sup>2</sup> | K <sub>2</sub> h <sup>2</sup> |
| W-1        | 35.6             | 27.6             | 24.5              | 21.4             | 0.0               | 0.0               | 42.9                          | 43.8                          | 24.6                          | 13.3                          |
| W-2        | 24.4             | 11.5             | 10.6              | 5.4              | 0.0               | 0.0               | 22.1                          | 15.0                          | 7.7                           | 14.5                          |
| W-3        | 4.4              | 1.1              | 3.2               | 3.6              | 0.0               | 0.0               | 0.0                           | 0.0                           | 1.5                           | 0.0                           |
| W-4        | 6.7              | 5.8              | 5.3               | 3.6              | 0.0               | 2.5               | 10.4                          | 7.5                           | 4.6                           | 2.4                           |
| W-5        | 0.0              | 1.1              | 0.0               | 0.0              | 10.3              | 22.5              | 3.9                           | 3.8                           | 6.2                           | 3.6                           |
| M-1        | 4.4              | 6.9              | 12.8              | 10.7             | 3.4               | 0.0               | 1.3                           | 3.8                           | 9.2                           | 6.0                           |
| M-2        | 6.7              | 1.1              | 3.2               | 3.6              | 0.0               | 5.0               | 3.9                           | 1.3                           | 4.6                           | 0.0                           |
| M-4        | 0.0              | 0.0              | 0.0               | 0.0              | 20.7              | 20.0              | 0.0                           | 0.0                           | 6.2                           | 3.6                           |
| VM-1       | 0.0              | 13.8             | 12.8              | 10.7             | 31.0              | 12.5              | 0.0                           | 1.3                           | 0.0                           | 0.0                           |
| VM-2       | 4.4              | 17.2             | 12.8              | 7.1              | 10.3              | 27.5              | 1.3                           | 3.8                           | 0.0                           | 0.0                           |
| VM-3       | 0.0              | 2.3              | 1.1               | 1.8              | 3.4               | 5.0               | 1.3                           | 1.3                           | 9.2                           | 12.0                          |
| VM-4       | 0.0              | 0.0              | 0.0               | 0.0              | 0.0               | 0.0               | 0.0                           | 2.5                           | 9.2                           | 26.5                          |
| M-3        | 0.0              | 0.0              | 1.1               | 0.0              | 0.0               | 2.5               | 1.3                           | 1.3                           | 0.0                           | 0.0                           |
| E-3        | 4.4              | 6.9              | 4.3               | 10.7             | 17.2              | 2.5               | 0.0                           | 0.0                           | 1.5                           | 3.6                           |
| E-2        | 6.7              | 4.6              | 7.4               | 16.1             | 3.4               | 0.0               | 11.7                          | 15.0                          | 1.5                           | 3.6                           |
| E-1        | 0.0              | 0.0              | 0.0               | 0.0              | 0.0               | 0.0               | 0.0                           | 0.0                           | 12.3                          | 9.6                           |

K<sub>1</sub>d: Didao Formation; K<sub>1</sub>ch: Chengzihe Formation; K<sub>1</sub>m: Muling Formation; K<sub>1</sub>dn: Dongshan Formation. K<sub>2</sub>h<sup>1</sup>: lower Houshigou Formation; K<sub>2</sub>h<sup>2</sup>: upper Houshigou Formation.

**Eastern migration of crustal uplift (early to middle syn-rift stages):** From the deposition of the Didao to Chengzihe formations, the data show that the source material from the Zhangguangcai Range (provenances W-1 to W-4) decreased significantly, while the contribution from the western Jiamusi Massif (provenance M-1) increased (Figure 8a-I, II). This change reveals the eastern migration of the crustal uplift from the Zhangguangcai Range to the western Jiamusi Massif (Figure 9a,b). Furthermore, from the Chengzihe to Muling formations, the material supply from the western provenances (provenances W-1 to W-4 and M-1) decreased (Figure 8b-I), while that from the eastern provenances (provenances E-2 and E-3) increased (Figure 8b-II), indicating further eastward migration of the crustal uplift (Figure 9b,c). Coeval igneous rocks (provenances VM-1 and VM-2) provided a large amount of detritus for the Boli Basin during the middle syn-rift stage (Figure 8b-III), implying that the magmatism was closely related to the evolution of the basin (Figure 9a-c). In summary, the crustal uplift of the Boli Basin was characterized by eastward migration and accompanied by coeval magmatism from the early to middle syn-rift stages.

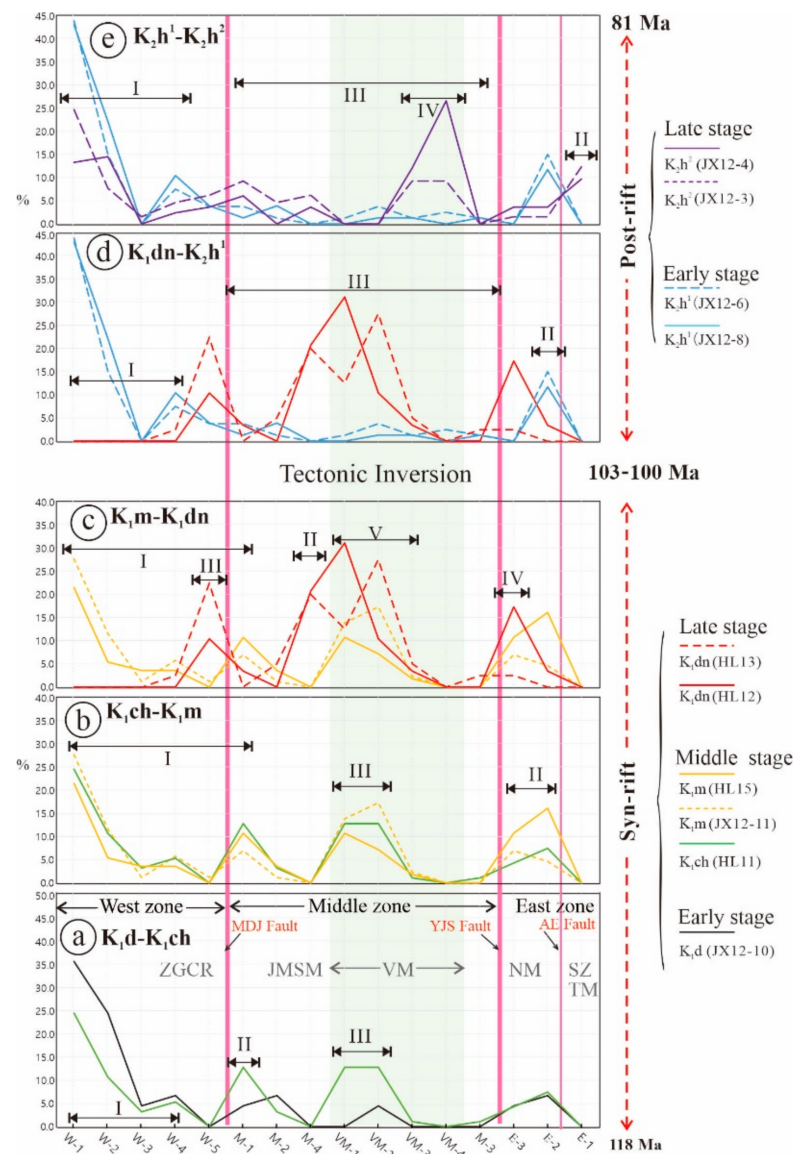


**Figure 8.** Line charts of contribution percentage of potential provenances to the Late Mesozoic clastic rocks in the Boli Basin. Variation in contribution percentage of potential provenances from (a) early to middle syn-rift stage, (b) middle syn-rift stage, (c) middle to late syn-rift stage, (d) late syn-rift stage to early post-rift stage and (e) early to late post-rift stage, respectively.

**Destruction of the Great Sanjiang Basin Group (late syn-rift stage):** At the late syn-rift stage of the basin when the Dongshan Formation formed, material provided from the western areas (provenances W-1 to W-4 and M-1) was insignificant, except for provenance W-5 (Figure 8c-I), revealing a significant reduction in the paleogeographic height of the western ranges. Materials from provenances W-5 (490–410 Ma) and M-4 (550–490 Ma) began to be eroded and transported into the Boli Basin at the first time point (Figure 8c-II,III). These Paleozoic rocks were generally considered to be seated at the middle-lower crust, containing different types of metamorphic rocks, such as schist, amphibolite, gneiss, and granulite, and parts of them represent the basement of the Jiamusi Massif [83,114–118,141–145]. These indicate that the middle-lower crust might have risen to the surface during the late syn-rift stage, which is considered to be related to the exhumation of the Hengshan, Mishan, and Huanan uplifts (Figure 9d). It is interesting to note that the contribution from M-4 is more significant than that of M-2, although both of them are developed in the uplift zone. This may be a result of the topography of the tilted fault block and the distribution characteristics of potential provenance. It is most likely that the clastic material of the samples of Dongshan Formation in the study area was derived from the Huanan uplift in the north of the Boli basin (Figure 1e). M-4, located near the basin boundary (Figure 5), with high topography, would contribute more material compared to M-2, which is further away from the basin and might be situated at a back slope of tilted fault block [161–163]. Moreover, it is noteworthy that material inputs from provenances W-5 and E-3 increased (Figure 8c-III,IV). Both of them are located on the outside of the boundary faults of the Great Sanjiang Basin Group (W-5 to the west of the Mudanjiang fault and E-3 to the east of the Yuejinshan fault; Figures 5 and 9d), revealing that the crust was exhumed along the boundary faults in an extensional environment. Additionally, material contribution from the coeval igneous rocks (provenances VM-1 to VM-3) significantly increased (Figure 8c-V). In summary, the basement of the Jiamusi Massif was uplifted to the surface during the deposition of the Dongshan Formation due to the continuous extension. The Great Sanjiang Basin Group (once unified basin) was segregated into a series of small basins, including the Hegang, Sanjiang, Jiamusi, Shuangyashan, Shuanghua, Hulin, Boli, and Jixi basins. These basins were isolated by several uplifts, such as the Hengshan, Mishan, and Huanan uplifts (Figure 9d).

**Western crustal uplift (early post-rift stage):** During the early post-rift stage, when the lower Houshigou Formation was deposited, the material supply from the Zhangguangcai Range (W-1 to W-4) increased tremendously (Figure 8d-I) and the detrital material from the eastern area (Nadanhada Massif) became significant (Figure 8d-II), while the contribution from the Jiamusi Massif (provenances M-1 to M-4 and VM-1 to VM-3) declined drastically (Figure 8d-III). These changes indicate the intense uplift of the crust in the west (slight in the east) and the subsidence of the basin-forming area during the early post-rift stage (Figure 9e). Seismic profiles and field investigations suggest that the tectonic inversion took place between the Dongshan and Houshigou formations, resulting in the formation of numerous compressional structures [55,158,164]. The compressional event might cause the revival of faults along the basin margin and the uplift of the Zhangguangcai Range and the Nadanhada Massif. Moreover, bimodal magmatism of ~100 Ma immediately developed on the Great Sanjiang Basin Group after the tectonic inversion [76,77], revealing that an extensional environment dominated this area after tension release, leading to basin subsidence. In general, we suggest that the crustal uplift in the western and eastern areas of the basin and the subsidence of the basin region resulted from a combination of tectonic inversion (~103–100 Ma) and the right after extension (~100–95 Ma).

**Formation of the eastern Coastal Ranges (late post-rift stage):** In the late post-rift stage, during which the upper Houshigou Formation was deposited, material contribution from the western provenances declined (Figure 8e-I), but detrital material coming from the most eastern area (provenance E-1) can be recognized in the Boli Basin (Figure 8e-II). This source change may indicate an eastward migration of the crustal uplift (Figure 9f). Since the E-1 is seated in the coastal areas of the Samarka, Zhuravlevka-Amur, and Taukha

Massifs (Figure 5), far from the Great Sanjiang Basin Group, we propose that the eastern Coastal Ranges were uplifted to a considerable height (Figure 9f), which is consistent with the results of previous studies in the Sanjiang and Hegang basins [71,72]. In addition, contribution of the middle provenances (M-1 to M-4) and part of the coeval igneous provenances (VM-3 and VM-4) increased (Figure 8e-III, IV), indicating that the eastward migration of the crustal uplift went through the Jiamusi Massif. In summary, the late post-rift stage was marked by the significant eastward migration of the crustal uplift and the formation of the eastern Coastal Ranges.

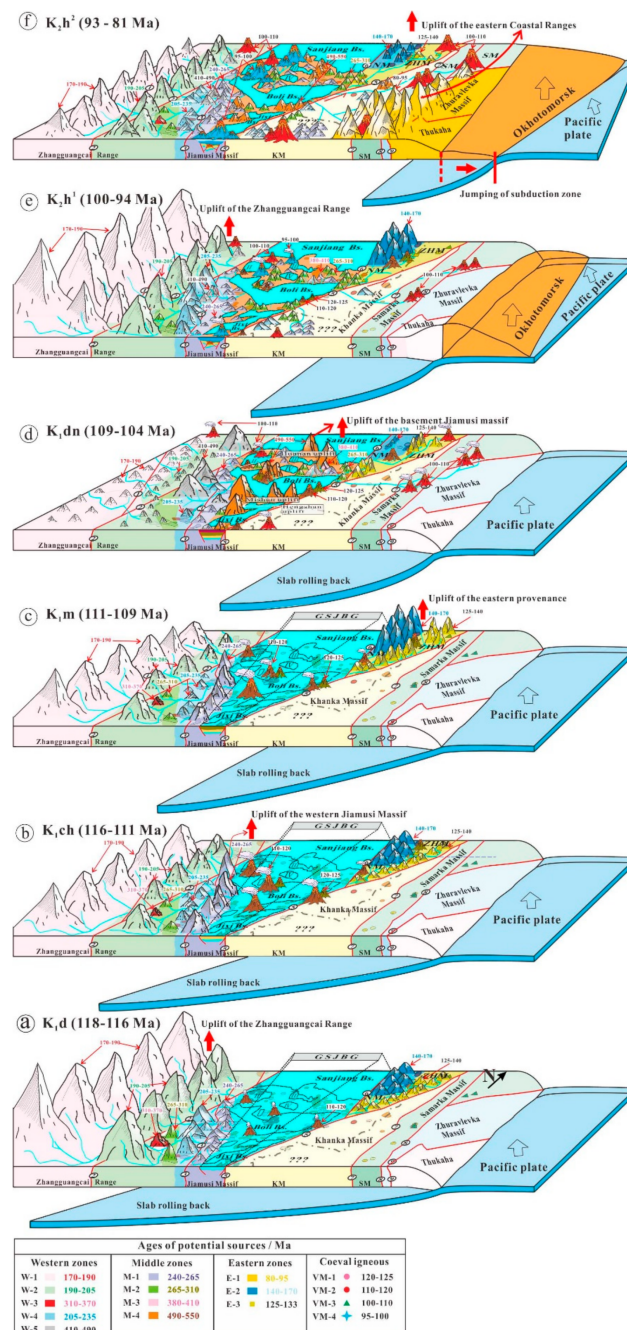


**Figure 9.** Sketch model of the crustal uplift and migration in the area of eastern NE China: (a) early syn-rift stage, Zhangguangcai Range uplift; (b,c) early to middle syn-rift stage, uplift areas migrated eastwards beginning from the region near the Mudanjiang fault to the Nadanhada massif; (d) late syn-rift stage, uplift of the Jiamusi massif; (e) early post-rift stage, uplift of the Zhangguangcai Range; (f) late post-rift stage, uplift of the eastern Coastal Ranges.

### 5.3. Tectonic Implications

As shown above, the Great Sanjiang Basin Group experienced a complex basin-range evolution during the Late Mesozoic, such as the eastward migration of crustal uplift, coeval volcanic-magmatism, tectonic inversion, and formation of the coastal range. The geodynamic settings related to the above processes depend on the complex tectonic evolution in NE China, which includes the closure of the Mongolian-Okhotsk Ocean [165,166], subduction and rolling back of the subducted slab of Paleo-Pacific Ocean and eastward migration of the trench [75,76], docking of the Okhotomorsk block along the continental margin of East Asia and the subsequent jumping of the subduction zone [39,167,168], and mantle upwelling caused by Paleo-Pacific subduction or the extrusion of the Okhotsk oceanic plateau [169,170].

**Slab rolling back in the syn-rift stage:** We show above that the spatio-temporal evolution of the crustal uplift during the syn-rift (118–104 Ma) was characterized by an eastward migration. This is consistent with the eastward migration of the magmatism in Northeast Asia [53,75,76]. It is generally believed that the lateral flow of the asthenosphere, induced by rolling back of the subducted Paleo-Pacific slab, controlled the eastward migration of the magmatism. However, whether or not formation of the basins in NE China migrated eastwards has been little studied. The Songliao basin, being the largest Late Mesozoic terrestrial sedimentary basin in NE China, is located in the west of the Great Sanjiang Basin Group (Figure 1b). Recent studies have established a detailed age frame for the basin formation by means of radiometric dating on volcanic, tephra, and clastic rocks both from drill cores and field outcrops, mostly based on zircon U-Pb dating methods. The volcanic rocks of the Huoshiling Formation formed between 131 Ma and 125 Ma [171–173] and the Shahezi Formation was deposited from 118 Ma to 114 Ma, based on the dating results of tephra [174,175]. In addition, a floating astronomical time scale (floating ATS) was established, and a duration of 11.14 Ma was proposed for the Shahezi Formation [176], suggesting that the deposition could extend to ~125 Ma, which is consistent with the youngest volcanic rocks of the Huoshiling Formation. Volcanic rocks of the Yingcheng Formation erupted at 114–112 Ma [48,171,172,177], and the zircon U-Pb ages of volcanic rocks from the upper sequence constrained the end time of the Yingcheng Formation to ~103 Ma [177]. These results demonstrated that the Songliao Basin and the Great Sanjiang Basin Group had similar tectonic evolution processes during the syn-rift period, but initial depositions of the sedimentary sequences in the Great Sanjiang Basin Group started later than those in the Songliao Basin. For instance, in the early syn-rift stage, magmatism and sedimentation developed in 131–125 Ma (Huoshiling Formation) and 118–116 Ma (Didao Formation); in the middle syn-rift stage, sedimentation accompanied with tephra interlayers formed in 125–114 Ma (Shahezi Formation) and 116–109 Ma (Chengzihe and Muling formations); in the late syn-rift stage, volcanic rocks with minor sedimentation developed in 114–103 Ma (Yingcheng Formation) and 109–104 Ma (Dongshan Formation).

In summary, during the syn-rift stage, the Great Sanjiang Basin Group underwent similar processes to the Songliao Basin, but not synchronously. This phenomenon is likely a result of the rolling back of the western Paleo-Pacific slab during this period (Figure 9a–c). The rolling back triggered the eastward lateral flow of the asthenosphere, which in turn heated the lower lithosphere beneath the Songliao Basin and the Great Sanjiang Basin Group, resulting in the eastward migration of lithospheric extension, magmatism, basin formation, and crustal uplift.

**Basin destruction:** Detrital zircon ages of the Dongshan Formation in the Boli Basin suggest that the basement uplift of the Jiamusi Massif occurred during the deposition of this formation. The transgression intermittently extended through the Great Sanjiang Basin Group during the deposition of the Didao and Muling formations (118–109 Ma). It is noteworthy that this transgression was not hindered by the Mishan, Hengshan, and Huanan uplifts in the Great Sanjiang Basin Group, but no longer continued during the period of the Dongshan Formation (109–104 Ma) [63]. Seismic profiles have revealed that the Didao to Dongshan formations (118–104 Ma) formed in an extensional environment [55],

which is consistent with the uplift time of the Zhangguangcai Range (118–102 Ma) obtained from the apatite fission track dating [28].

The rolling back of the subducted Paleo-Pacific slab may result in extensional destruction of the Great Sanjiang Basin Group and its late formation compared to the Songliao Basin. However, it is still unclear why the Songliao Basin and the Great Sanjiang Basin Group have different initiation times, but share consistent termination of the syn-rift stage at 104–103 Ma. Previous studies have revealed a dramatic tectonic inversion (compression) in the Great Sanjiang Basin Group after the syn-rift by combining seismic profiles and field observations, showing a much steeper dip in the sequences of the syn-rift than those of the post-rift [72,158]. Moreover, the entirety of NE China, including the Great Sanjiang Basin Group, Songliao basin, and the Western Basin Group, responded to this tectonic inversion, which was interpreted to be related to the docking of the Okhotomorsk block along the continental margin of East Asia (Figure 9e) [39,55,167,178]. From a broader geographical perspective, the NW-NE crustal shortening in the middle Cretaceous resulted in the formation of a large number of basin-range and rapid exhumation events in eastern China [179–182], and the formation of the eastern Coastal Ranges, as well [183–185]. These topographic variations also led to arid climate or deserts in eastern East Asia [14,186,187].

The docking time of the Okhotomorsk block along the eastern continental margin of Eurasia, however, remains controversial. In NE China, the compression event developed in 103–89 Ma based on studies of detrital zircon ages [48,55,71,167,178], while the peak period of 89–87 Ma was determined by apatite fission track dating in the Great Xing'an Range [181]. Studies of seismic profiles and field investigations have suggested that the compression event may have lasted until 79–65 Ma [188–190]. However, the time of the compressional events was constrained to 100–90 Ma based on studies on the basins in the North China Block [179,191,192]. It has been suggested that the Coastal Ranges were formed in 115–110 Ma in the South China Block, but in 100–89 Ma in NE China [184]. In general, the compression event in northern China was limited to 103–87 Ma. However, the accretion of the Okhotomorsk block to the eastern margin of the Siberian block was in 93–89 Ma [193], indicating that its collage with the southern micro-continents, e.g., NE China, should be earlier than 93 Ma. In addition, the termination of the syn-rift stage in the Great Sanjiang Basin Group and the Songliao Basin was ~104–103 Ma, constraining the tectonic inversion in NE China to mostly occur in 103–93 Ma. Furthermore, bimodal magmatism in the Great Sanjiang Basin Group was well developed in 100–95 Ma [76–80,156,159], revealing an intense extensional rather than compressional environment.

In conclusion, the initial destruction of the Great Sanjiang Basin Group occurred during the deposition of the Dongshan Formation (109–104 Ma), likely related to the persistent extension during the syn-rift stage (118–104 Ma) induced by the slab rolling back (Figure 9a–d). The tectonic inversion caused by the Okhotomorsk block collision was more likely in ~103–101 Ma, which was an extremely rapid but intense compressional event leading to the second destruction of the Great Sanjiang Basin Group.

**Jumping of subduction zone in the post-rift stage:** Studies on the detrital zircon ages of the Boli Basin revealed uplift of the eastern Coastal Ranges (Figures 8e and 9e,f). The 95–80 Ma felsic magmatic rocks (granite, dacite, monzogranite, and rhyolite) of the Samarka, Zhuravlevka-Amur, and Taukha massifs in the Russia's Primorskiy Krai area provide material supplied to the basin filling of the Great Sanjiang Basin Group [146–149]. In addition, numerous Cretaceous basins are located in the southern Korean Peninsula, for instance the Gyeongsang Basin, which is the largest one. The Yuncheon Group of this basin mainly consists of volcanic rocks (92–82 Ma) [194–199] and tephra (90–84 Ma) [198,200]. Moreover, previous studies have shown that this magmatism developed in a sinistral strike-slip environment accompanied by the formation of pull-apart basins and high volcanic platforms [200–202]. In summary, previous studies in Russia's Primorskiy Krai and the southern Korean Peninsula suggest that in 95–80 Ma, volcanic-magmatism was developed and accompanied by the crustal uplift.

In comparison with the magmatism of the syn-rift stage (~120–100 Ma), which was mainly distributed in the interior of the Great Sanjiang Basin Group and its periphery, post-rift magmatism (~100–80 Ma) is characterized by oceanward migration. It is noteworthy that the Khanka Massif, located between the Great Sanjiang Basin Group and the eastern coastal magmatic belt (Figure 5), hardly developed coeval magmatism, suggesting oceanward receding magmatism in discrete jumps. It has been suggested that excessive accretionary prism growth can force a retreat of the arc-trench system, and that the arc formation follows the oceanward receding trench in discrete jumps, forming trenchward younging magmatism [54]. Considering that the amalgamation of the Okhotomorsk block along the eastern continental margin of Eurasia had a similar scene to the above-mentioned processes, we tentatively propose that a trench jump from the western edge of the Okhotomorsk block to the eastern side might have occurred, resulting in trenchward younging magmatism in discrete jumps (Figure 9e,f). The volcanic arc platform forming near the coast ensures debris to be transported to the Great Sanjiang Basin Group when the upper Houshigou Formation was deposited. Namely, the formation of the eastern Coastal Ranges revealed by the detrital zircons of the Boli Basin is closely related to the jumping of the subduction zone caused by the collision of the Okhotomorsk block [168].

## 6. Conclusions

On the basis of the detrital zircon age distribution patterns of the Late Mesozoic clastic rocks and previously reported results, the formation of the sedimentary sequences and multiple-stage evolution of the Boli Basin can be proposed as follows: the early syn-rift stage formed the Didao Formation (118–116 Ma), the middle syn-rift stage deposited the Chengzihe Formation (116–111 Ma) and the Muling Formation (111–109 Ma), and the late syn-rift stage formed the Dongshan Formation (109–104 Ma). After the tectonic inversion at ~103–101 Ma, the Houshigou Formation deposited during the post-rift stage (lower section of ~100–94 Ma, upper section of 93–81 Ma or later).

The Boli Basin and its periphery experienced four stages of crustal uplift, i.e., the eastward migration of the crustal uplift during the early and middle syn-rift stages (118–109 Ma); exhumation of the basement of the Jiamusi Massif and destruction of the Great Sanjiang Basin Group during the late syn-rift stage (109–104 Ma); uplift of the Zhangguangcai Range during the early post-rift stage (~100–94 Ma); and uplift of the eastern Coastal Ranges during the late post-rift stage (93 Ma to 81 Ma or later).

Tectonic evolution of the Great Sanjiang Basin Group in eastern NE China during the Late Mesozoic is jointly controlled by the Paleo-Pacific plate subduction and the Okhotomorsk block movement. The eastward migration crustal uplift during the early and middle syn-rift stages was closely related to the rolling back of the Paleo-Pacific slab. The first destruction of the basin under an extensional environment during the late syn-rift stage resulted from the persistent rolling back process. The second destruction of the basin under a compression environment was caused by the tectonic inversion related to the docking of the Okhotomorsk block along the East-Asia continental margin. The formation of the eastern Coastal Ranges was controlled by jumping of the subduction zone due to the collision of the Okhotomorsk block.

For the rift basins with abundant volcanic and plutonic rocks, synthesizing the age data of clastic rocks and igneous rocks is beneficial for dating sedimentary series. In combination with the probability density and kernel density estimations of detrital zircon U-Pb ages, the line charts of percentages of source contributions are more conducive to revealing the spatio-temporal differences in crustal uplift, especially for basins having complex tectonic or orogenic processes.

**Supplementary Materials:** The following are available online at <https://www.mdpi.com/article/10.3390/min12091166/s1>, Table S1: Detrital zircon U-Pb dating results of Late Mesozoic clastic rocks from the Boli basin, eastern NE China.

**Author Contributions:** Writing—original draft preparation, S.H.; writing—review and editing, S.L., H.C. and F.C.; visualization, C.C. and J.H.; supervision, F.C. All authors have read and agreed to the published version of the manuscript.

**Funding:** This study was supported by the National Natural Science Foundation of China, grant No. 41872049, and the National Key R&D Program of China, grant No. 2016YFC0600404.

**Data Availability Statement:** The authors confirm that the data supporting the findings of this study are available within the article and its Supplementary Materials.

**Acknowledgments:** We gratefully thank Z.-H. Hou and P. Xiao for their assistance during analytical work. Constructive suggestions and comments from two anonymous reviewers have greatly improved the manuscript. A special acknowledgement goes to the China Scholarship Council who covers my maintenance at Heidelberg University.

**Conflicts of Interest:** The authors declare no conflict of interest.

## References

- Zhang, Q.; Song, M.; Ding, Z.; Guo, M.; Zhou, M.; Dai, C.; Hou, G.; Zhang, P. Exhumation history and preservation of the Jiaojia giant gold deposit, Jiaodong Peninsula. *Sci. China Earth Sci.* **2002**, *65*, 1161–1177. [[CrossRef](#)]
- Liu, S.; Zhang, G. Fundamental ideas, contents and methods in study of basin and mountain relationships. *Earth Sci. Front.* **2005**, *12*, 101–111.
- Lin, W.; Wei, W. Late Mesozoic extensional tectonics in the North China Craton and its adjacent regions: A review and synthesis. *Int. Geol. Rev.* **2020**, *62*, 811–839. [[CrossRef](#)]
- Mao, J.W. Mesozoic large-scale metallogenic pulses in North China and corresponding geodynamic settings. *Acta Petrol. Sin.* **2005**, *21*, 169–188.
- Allen, P.A. From landscapes into geological history. *Nature* **2008**, *451*, 274–276. [[CrossRef](#)] [[PubMed](#)]
- Whittaker, A.C. How do landscapes record tectonics and climate? *Lithosphere* **2012**, *4*, 160–164. [[CrossRef](#)]
- Ferraccioli, F.; Finn, C.A.; Jordan, T.A.; Bell, R.E.; Anderson, L.M.; Damaske, D. East Antarctic rifting triggers uplift of the Gamburtsev Mountains. *Nature* **2011**, *479*, 388–392. [[CrossRef](#)]
- King, G.; Ellis, M. The origin of large local uplift in extensional regions. *Nature* **1990**, *348*, 689–693. [[CrossRef](#)]
- Bao, X.; Eaton, D.W.; Guest, B. Plateau uplift in western Canada caused by lithospheric delamination along a craton edge. *Nat. Geosci.* **2014**, *7*, 830–833. [[CrossRef](#)]
- Andersen, J.; Göğüş, O.H.; Pysklywec, R.N.; Santimano, T.; Şengül Uluocak, E. Symptomatic lithospheric drips triggering fast topographic rise and crustal deformation in the Central Andes. *Commun. Earth Environ.* **2022**, *3*, 150. [[CrossRef](#)]
- Göğüş, O.H.; Pysklywec, R.N.; Şengör, A.M.C.; Gün, E. Drip tectonics and the enigmatic uplift of the Central Anatolian Plateau. *Nat. Commun.* **2017**, *8*, 1538. [[CrossRef](#)] [[PubMed](#)]
- Perkins, J.P.; Ward, K.M.; De Silva, S.L.; Zandt, G.; Beck, S.L.; Finnegan, N.J. Surface uplift in the Central Andes driven by growth of the Altiplano Puna Magma Body. *Nat. Commun.* **2016**, *7*, 13185. [[CrossRef](#)] [[PubMed](#)]
- Yu, J.; Zheng, D.; Pang, J.; Li, C.; Wang, Y.; Wang, Y.; Hao, Y.; Zhang, P. Cenozoic mountain building in eastern China and its correlation with reorganization of the Asian climate regime. *Geology* **2022**, *50*, 859–863. [[CrossRef](#)]
- Zhang, J.; Liu, Y.; Flögel, S.; Zhang, T.; Wang, C.; Fang, X. Altitude of the East Asian Coastal Mountains and their influence on Asian climate during Early Late Cretaceous. *J. Geophys. Res. Atmos.* **2021**, *126*, e2020JD034413. [[CrossRef](#)]
- Bishop, P. Long-term landscape evolution: Linking tectonics and surface processes. *Earth Surface Processes and Landforms: J. Br. Geomorphol. Res. Group* **2007**, *32*, 329–365. [[CrossRef](#)]
- Singer, B.S.; Le Mével, H.; Licciardi, J.M.; Córdova, L.; Tikoff, B.; Garibaldi, N.; Andersen, N.L.; Diefenbach, A.K.; Feigl, K.L. Geomorphic expression of rapid Holocene silicic magma reservoir growth beneath Laguna del Maule, Chile. *Sci. Adv.* **2018**, *4*, eaat1513. [[CrossRef](#)]
- Jamtveit, B.; Ben-Zion, Y.; Renard, F.; Austrheim, H. Earthquake-induced transformation of the lower crust. *Nature* **2018**, *556*, 487–491. [[CrossRef](#)]
- Antonelli, A.; Kissling, W.D.; Flantua, S.G.; Bermúdez, M.A.; Mulch, A.; Muellner-Riehl, A.N.; Kreft, H.; Linder, H.P.; Badgley, C.; Fjeldså, J.; et al. Geological and climatic influences on mountain biodiversity. *Nat. Geosci.* **2018**, *11*, 718–725. [[CrossRef](#)]
- Li, T.D. The uplifting process and mechanism of the Qinghai-Tibet plateau. *Acta Geosci. Sin.* **1995**, *1*, 1–9.
- McKenzie, D. A possible mechanism for epeirogenic uplift. *Nature* **1984**, *307*, 616–618. [[CrossRef](#)]
- Tang, G.J.; Wyman, D.A.; Wang, Q.; Yin, J.Y.; Dan, W. Long-Distance Lateral Magma Propagation and Pamir Plateau Uplift. *Geophys. Res. Lett.* **2022**, *49*, e2021GL096467. [[CrossRef](#)]
- Wolf, S.G.; Huisman, R.S.; Braun, J.; Yuan, X. Topography of mountain belts controlled by rheology and surface processes. *Nature* **2022**, *606*, 516–523. [[CrossRef](#)] [[PubMed](#)]
- Zheng, H.; Sun, X.; Zhu, D.; Tian, J.; He, S.; Wang, Y.; Zhang, X. The structural characteristics, age of origin, and tectonic attribute of the Erguna Fault, NE China. *Sci. China Earth Sci.* **2015**, *58*, 1553–1565. [[CrossRef](#)]

24. Sun, X.M.; Zhang, X.Q.; He, S.; Wang, P.J.; Zheng, H.; Wan, K.; Li, D.Z. Two important Cretaceous deformation events of the Dunhua-Mishan Fault Zone, NE China. *Acta Petrol. Sin.* **2016**, *32*, 1114–1128.
25. Zhang, X.D.; Yu, Q.; Chen, F.J.; Wang, X.W. Structural characteristics, origin and evolution of metamorphic core complex in central basement uplift and Xujiaweizi faulted depression in Songliao basin, northeast China. *Earth Sci. Front.* **2000**, *7*, 411–419.
26. Dou, J.Z.; Fu, S.; Zhang, H.F. Consolidation and cooling paths of the Guojialing granodiorites in Jiaodong Peninsula: Implication for crustal uplift and exhumation. *Acta Petrol. Sin.* **2015**, *31*, 2325–2336.
27. He, S.; Li, X.H.; Zhang, H.F.; Li, S.Q.; Chen, F. Constraints of zircon U-Pb and biotite Rb-Sr ages and P-T conditions on the emplacement and uplifting of the Late Mesozoic Jinan gabbro, eastern North China. *J. Asian Earth Sci.* **2019**, *183*, 103972. [[CrossRef](#)]
28. Wang, N.; Zhang, Z.; Malusà, M.G.; Wu, L.; Chew, D.; Zhang, J.; Xiang, D.; Xiao, W. Pulsed Mesozoic exhumation in Northeast Asia: New constraints from zircon U-Pb and apatite U-Pb, fission track and (U-Th)/He analyses in the Zhangguangcai Range, NE China. *Tectonophysics* **2021**, *818*, 229075. [[CrossRef](#)]
29. Kasanzu, C.H. Apatite fission track and (U-Th)/He thermochronology from the Archean Tanzania Craton: Contributions to cooling histories of Tanzanian basement rocks. *Geosci. Front.* **2017**, *8*, 999–1007. [[CrossRef](#)]
30. Wu, L.; Wang, F.; Yang, J.; Wang, Y.; Zhang, W.; Yang, L.; Shi, W. Meso-Cenozoic uplift of the Taihang Mountains, North China: Evidence from zircon and apatite thermochronology. *Geol. Mag.* **2020**, *157*, 1097–1111. [[CrossRef](#)]
31. Huyghe, D.; Mouthereau, F.; Segalen, L.; Furió, M. Long-term dynamic topographic support during post-orogenic crustal thinning revealed by stable isotope ( $\delta^{18}\text{O}$ ) paleo-altimetry in eastern Pyrenees. *Sci. Rep.* **2020**, *10*, 2267. [[CrossRef](#)] [[PubMed](#)]
32. Zhang, L.; Wang, C.; Cao, K.; Wang, Q.; Tan, J.; Gao, Y. High elevation of Jiaolai Basin during the Late Cretaceous: Implication for the coastal mountains along the East Asian margin. *Earth Planet. Sci. Lett.* **2016**, *456*, 112–123. [[CrossRef](#)]
33. Dickinson, W.R.; Suczek, C.A. Plate tectonics and sandstone compositions. *Aapg Bull.* **1979**, *63*, 2164–2182.
34. Roser, B.P.; Korsch, R.J. Provenance signatures of sandstone-mudstone suites determined using discriminant function analysis of major-element data. *Chem. Geol.* **1988**, *67*, 119–139. [[CrossRef](#)]
35. Bhatia, M.R. Rare earth element geochemistry of Australian Paleozoic graywackes and mudrocks: Provenance and tectonic control. *Sediment. Geol.* **1985**, *45*, 97–113. [[CrossRef](#)]
36. Bhatia, M.R. Plate tectonics and geochemical composition of sandstones. *J. Geol.* **1983**, *91*, 611–627. [[CrossRef](#)]
37. Bhatia, M.R.; Crook, K.A. Trace element characteristics of graywackes and tectonic setting discrimination of sedimentary basins. *Contrib. Mineral. Petrol.* **1986**, *92*, 181–193. [[CrossRef](#)]
38. Bhatia, M.R. Composition and classification of Paleozoic flysch mudrocks of eastern Australia: Implications in provenance and tectonic setting interpretation. *Sediment. Geol.* **1984**, *41*, 249–268. [[CrossRef](#)]
39. Li, S.Q.; He, S.; Chen, F. Provenance changes across the mid-Cretaceous unconformity in basins of northeastern China: Evidence for an integrated paleolake system and tectonic transformation. *GSA Bull.* **2021**, *133*, 185–198. [[CrossRef](#)]
40. Chen, F.; Zhu, X.Y.; Wang, W.; Wang, F.; Hieu, P.T.; Siebel, W. Single-grain detrital muscovite Rb-Sr isotopic composition as an indicator of provenance for the Carboniferous sedimentary rocks in northern Dabie, China. *Geochem. J.* **2009**, *43*, 257–273. [[CrossRef](#)]
41. Scott, E.M.; Allen, M.B.; Macpherson, C.G.; McCaffrey, K.J.; Davidson, J.P.; Saville, C.; Ducea, M.N. Andean surface uplift constrained by radiogenic isotopes of arc lavas. *Nat. Commun.* **2018**, *9*, 969. [[CrossRef](#)] [[PubMed](#)]
42. Belousova, E.A.; Griffin, W.L.; O'Reilly, S.Y.; Fisher, N.L. Igneous zircon: Trace element composition as an indicator of source rock type. *Contrib. Mineral. Petrol.* **2002**, *143*, 602–622. [[CrossRef](#)]
43. Hoskin, P.W.; Ireland, T.R. Rare earth element chemistry of zircon and its use as a provenance indicator. *Geology* **2000**, *28*, 627–630. [[CrossRef](#)]
44. Veevers, J.J.; Saeed, A.; Belousova, E.A.; Griffin, W.L. U-Pb ages and source composition by Hf-isotope and trace-element analysis of detrital zircons in Permian sandstone and modern sand from southwestern Australia and a review of the paleogeographical and denudational history of the Yilgarn Craton. *Earth-Sci. Rev.* **2005**, *68*, 245–279. [[CrossRef](#)]
45. Lease, R.O.; Burbank, D.W.; Gehrels, G.E.; Wang, Z.; Yuan, D. Signatures of mountain building: Detrital zircon U/Pb ages from northeastern Tibet. *Geology* **2007**, *35*, 239–242. [[CrossRef](#)]
46. Yang, J.H.; Wu, F.Y.; Shao, J.A.; Wilde, S.A.; Xie, L.W.; Liu, X.M. Constraints on the timing of uplift of the Yanshan Fold and Thrust Belt, North China. *Earth Planet. Sci. Lett.* **2006**, *246*, 336–352. [[CrossRef](#)]
47. Cawood, P.A.; Hawkesworth, C.J.; Dhuime, B. Detrital zircon record and tectonic setting. *Geology* **2012**, *40*, 875–878. [[CrossRef](#)]
48. Li, S.Q.; Chen, F.; Siebel, W.; Wu, J.D.; Zhu, X.Y.; Shan, X.L.; Sun, X.M. Late Mesozoic tectonic evolution of the Songliao basin, NE China: Evidence from detrital zircon ages and Sr-Nd isotopes. *Gondwana Res.* **2012**, *22*, 943–955. [[CrossRef](#)]
49. Thomas, W.A. Detrital-zircon geochronology and sedimentary provenance. *Lithosphere* **2011**, *3*, 304–308. [[CrossRef](#)]
50. Gehrels, G. Detrital zircon U-Pb geochronology applied to tectonics. *Annu. Rev. Earth Planet. Sci.* **2014**, *42*, 127–149. [[CrossRef](#)]
51. Dickinson, W.R.; Gehrels, G.E. Use of U-Pb ages of detrital zircons to infer maximum depositional ages of strata: A test against a Colorado Plateau Mesozoic database. *Earth Planet. Sci. Lett.* **2009**, *288*, 115–125. [[CrossRef](#)]
52. Vermeesch, P. On the visualisation of detrital age distributions. *Chem. Geol.* **2012**, *312*, 190–194. [[CrossRef](#)]
53. Zhang, J.; Gao, S.; Ge, W.; Wu, F.; Yang, J.; Wilde, S.; Li, M. Geochronology of the Mesozoic volcanic rocks in the Great Xing'an Range, northeastern China: Implications for subduction-induced delamination. *Chem. Geol.* **2010**, *276*, 144–165. [[CrossRef](#)]

54. Gianni, G.M.; Luján, S.P. Geodynamic controls on magmatic arc migration and quiescence. *Earth-Sci. Rev.* **2021**, *218*, 103676. [[CrossRef](#)]
55. Zhang, F.Q.; Dilek, Y.; Chen, H.L.; Yang, S.F.; Meng, Q.A. Structural architecture and stratigraphic record of Late Mesozoic sedimentary basins in NE China: Tectonic archives of the Late Cretaceous continental margin evolution in East Asia. *Earth-Sci. Rev.* **2017**, *171*, 598–620. [[CrossRef](#)]
56. He, Z.; Liu, Z.; Zhang, X.; Chen, Y.; Dong, L. Subdivisions of structural layers and tectonic-sedimentary evolution of eastern basins in Heilongjiang in Late Mesozoic. *Glob. Geol.* **2009**, *28*, 20–27.
57. Jia, C.Z.; Zheng, M. Sedimentary history, tectonic evolution of Cretaceous Dasanjiang Basin in Northeast China and the significance of oil and gas exploration of its residual basins. *J. Daqing Pet. Inst.* **2010**, *34*, 1–12.
58. Wen, Q.; Liu, Y.; Li, J.; Bai, J.; Sun, X.; Zhao, Y.; Han, G. Provenance analysis and tectonic implications for the Cretaceous sandstones in the Jixi and Boli Basins, Heilongjiang. *Sediment. Geol. Tethyan Geol.* **2008**, *28*, 52–59.
59. Zhao, X.; Yang, S.; Chen, H.; Zhang, F.; Zhang, Y.; Yang, C.; Sun, M. Features of multistage Cretaceous conglomerate deposition and its palaeo-geographic significance in Jixi Basin of eastern Heilongjiang, NE China. *Acta Sci. Nat. Univ. Pekin.* **2012**, *48*, 419–432.
60. Cheng, J.H.; He, C.Q. Early Cretaceous dinoflagellates from the Didao Formation in the Jixi Basin, eastern Heilongjiang Province, NE China. *Acta Palaeontol. Sin.* **2001**, *40*, 132–140.
61. He, C.; Sun, X. Late Hauterivian dinoflagellates from the lower part of the Chengzihe Formation in Jixi Basin, eastern Heilongjiang, NE China. *Acta Palaeontol. Sin.* **2000**, *39*, 46–62.
62. Sha, J. Cretaceous stratigraphy of northeast China: Non-marine and marine correlation. *Cretac. Res.* **2007**, *28*, 146–170. [[CrossRef](#)]
63. Sha, J.; Hirano, H.; Yao, X.; Pan, Y. Late Mesozoic transgressions of eastern Heilongjiang and their significance in tectonics, and coal and oil accumulation in northeast China. *Palaeogeogr. Palaeoclimatol. Palaeoecol.* **2008**, *263*, 119–130. [[CrossRef](#)]
64. Sha, J.; Matsukawa, M.; Cai, H.; Jiang, B.; Ito, M.; He, C.; Gu, Z. The Upper Jurassic-Lower Cretaceous of eastern Heilongjiang, northeast China: Stratigraphy and regional basin history. *Cretac. Res.* **2003**, *24*, 715–728. [[CrossRef](#)]
65. Sha, J.; Wang, J.; Kirillova, G.; Pan, Y.; Cai, H.; Wang, Y.; Yao, X.; Peng, B. Upper Jurassic and lower cretaceous of Sanjiang-Middle Amur basin: Non-marine and marine correlation. *Sci. China Ser. D Earth Sci.* **2009**, *52*, 1873–1889. [[CrossRef](#)]
66. Wan, C.; Liao, X. Early Cretaceous Nonmarine Dinoflagellate Assemblages of Well 206 in Sanjiang Basin from Heilongjiang. *Chin. Sci. Abstr. Ser. B* **1995**, *2*, 49.
67. Yang, X. New material of fossil plants from the Early Cretaceous Muling Formation of the Jixi Basin, eastern Heilongjiang Province, China. *Acta Palaeontol. Sin.* **2003**, *42*, 561–584.
68. Yang, X.; He, C.; Li, W.; Piao, T. Marine dinoflagellates from Lower Cretaceous Muling Formation of Jixi basin, China and their palaeoenvironmental significance. *Chin. Sci. Bull.* **2003**, *48*, 2480–2483.
69. Zhu, Y.H.; He, C.Q. The Middle Jurassic to Early Cretaceous dinoflagellate assemblage sequence from eastern Heilongjiang. *J. Stratigr.* **2003**, *27*, 282–288.
70. Zhu, Y.; He, C. Middle Jurassic to Early Cretaceous dinoflagellate assemblage zones in eastern Heilongjiang Province, northeast China. *Cretac. Res.* **2007**, *28*, 327–332. [[CrossRef](#)]
71. Sun, M.; Chen, H.; Zhang, F.; Wilde, S.A.; Minna, A.; Lin, X.; Yang, S. Cretaceous provenance change in the Hegang Basin and its connection with the Songliao Basin, NE China: Evidence for lithospheric extension driven by palaeo-Pacific roll-back. *Geol. Soc. Lond. Spec. Publ.* **2015**, *413*, 91–117. [[CrossRef](#)]
72. Zhang, F.; Chen, H.; Batt, G.E.; Dilek, Y.; Min-Na, A.; Sun, M.; Yang, S.; Meng, Q.; Zhao, X. Detrital zircon U-Pb geochronology and stratigraphy of the Cretaceous Sanjiang Basin in NE China: Provenance record of an abrupt tectonic switch in the mode and nature of the NE Asian continental margin evolution. *Tectonophysics* **2015**, *665*, 58–78. [[CrossRef](#)]
73. Chen, D.; Zhang, F.; Tian, Y.; Zhou, Z.; Dilek, Y.; Chen, H.; Zhang, K.; Zhao, X. Timing of the late Jehol Biota: New geochronometric constraints from the Jixi Basin, NE China. *Palaeogeogr. Palaeoclimatol. Palaeoecol.* **2018**, *492*, 41–49. [[CrossRef](#)]
74. Liu, S. Palaeoenvironmental evolution of the Lower Cretaceous Dongshan Formation in the eastern Depression of the Boli Basin. Master's Thesis, Jilin University, Changchun, China, 2019.
75. Xu, W.L.; Pei, F.P.; Wang, F.; Meng, E.; Ji, W.Q.; Yang, D.B.; Wang, W. Spatial-temporal relationships of Mesozoic volcanic rocks in NE China: Constraints on tectonic overprinting and transformations between multiple tectonic regimes. *J. Asian Earth Sci.* **2013**, *74*, 167–193. [[CrossRef](#)]
76. Sun, M.; Chen, H.; Milan, L.A.; Wilde, S.A.; Jourdan, F.; Xu, Y. Continental arc and back-arc migration in Eastern NE China: New constraints on Cretaceous Paleo-Pacific subduction and rollback. *Tectonics* **2018**, *37*, 3893–3915. [[CrossRef](#)]
77. Sun, M.D.; Chen, H.L.; Zhang, F.Q.; Wilde, S.A.; Dong, C.W.; Yang, S.F. A 100 Ma bimodal composite dyke complex in the Jiamusi Block, NE China: An indication for lithospheric extension driven by Paleo-Pacific roll-back. *Lithos* **2013**, *162*, 317–330. [[CrossRef](#)]
78. Liu, K.; Wilde, S.A.; Zhang, J.; Xiao, W.; Wang, M.; Ge, M. Zircon U-Pb dating and whole-rock geochemistry of volcanic rocks in eastern Heilongjiang Province, NE China: Implications for the tectonic evolution of the Mudanjiang and Paleo-Pacific oceans from the Jurassic to Cretaceous. *Geol. J.* **2020**, *55*, 1866–1889. [[CrossRef](#)]
79. Zhang, L.; Han, B.F.; Zhu, Y.F.; Xu, Z.; Chen, J.F.; Song, B. Geochronology, mineralogy, crystallization process and tectonic implications of the Shuangyashan monzogabbro in eastern Heilongjiang Province. *Acta Petrol. Sin.* **2009**, *25*, 577–587.
80. Zhu, Z.P.; Liu, L.; Ma, R.; Qiu, Z.K.; Ma, S.H.  $^{40}\text{Ar}/^{39}\text{Ar}$  isotopic dating and geological significance of mafic rocks from the Jixi Basin, Heilongjiang Province. *J. Jilin Univ. (Earth Sci. Ed.)* **2009**, *39*, 238–243.

81. Ge, M.H.; Zhang, J.J.; Li, L.; Liu, K. A Triassic-Jurassic westward scissor-like subduction history of the Mudanjiang Ocean and amalgamation of the Jiamusi Block in NE China: Constraints from whole-rock geochemistry and zircon U-Pb and Lu-Hf isotopes of the Lesser Xing'an-Zhangguangcai Range granitoids. *Lithos* **2018**, *302*, 263–277.
82. Dong, Y.; Ge, W.C.; Yang, H.; Ji, Z.; He, Y.; Zhao, D.; Xu, W. Convergence history of the Jiamusi and Songnen-Zhangguangcai Range massifs: Insights from detrital zircon U-Pb geochronology of the Yilan Heilongjiang Complex, NE China. *Gondwana Res.* **2018**, *56*, 51–68. [[CrossRef](#)]
83. Wilde, S.; Wu, F.Y.; Zhang, X.Z. Late Pan-African magmatism in northeastern China: SHRIMP U-Pb zircon evidence from granitoids in the Jiamusi Massif. *Precambrian Res.* **2003**, *122*, 311–327. [[CrossRef](#)]
84. Wu, F.Y.; Sun, D.Y.; Ge, W.C.; Zhang, Y.B.; Grant, M.L.; Wilde, S.A.; Jahn, B.M. Geochronology of the Phanerozoic granitoids in northeastern China. *J. Asian Earth Sci.* **2011**, *41*, 1–30. [[CrossRef](#)]
85. Xu, B.; Zhao, P.; Wang, Y.; Liao, W.; Luo, Z.; Bao, Q.; Zhou, Y. The pre-Devonian tectonic framework of Xing'an-Mongolia orogenic belt (XMOB) in north China. *J. Asian Earth Sci.* **2015**, *97*, 183–196. [[CrossRef](#)]
86. Liu, Y.; Hu, Z.; Zong, K.; Gao, C.; Gao, S.; Xu, J.; Chen, H. Reappraisal and refinement of zircon U-Pb isotope and trace element analyses by LA-ICP-MS. *Chin. Sci. Bull.* **2010**, *55*, 1535–1546. [[CrossRef](#)]
87. Andersen, T. Correction of common lead in U-Pb analyses that do not report 204Pb. *Chem. Geol.* **2002**, *192*, 59–79. [[CrossRef](#)]
88. Ludwig, K.R. ISOPLOT3: A Geochronological Toolkit for Microsoft Excel. *Berkeley Geochronol. Cent. Spec. Publ.* **2003**, *4*, 74.
89. Ge, M.H.; Zhang, J.J.; Li, L.; Liu, K. Ages and geochemistry of Early Jurassic granitoids in the Lesser Xing'an-Zhangguangcai Ranges, NE China: Petrogenesis and tectonic implications. *Lithosphere* **2019**, *11*, 804–820. [[CrossRef](#)]
90. Ge, M.H.; Zhang, J.J.; Li, L.; Liu, K.; Ling, Y.Y.; Wang, J.M.; Wang, M. Geochronology and geochemistry of the Heilongjiang Complex and the granitoids from the Lesser Xing'an-Zhangguangcai Range: Implications for the late Paleozoic-Mesozoic tectonics of eastern NE China. *Tectonophysics* **2017**, *717*, 565–584. [[CrossRef](#)]
91. Hu, X.; Ding, Z.; He, M.; Yao, S.; Zhu, B.; Shen, J.; Chen, B. A porphyry-skarn metallogenic system in the Lesser Xing'an Range, NE China: Implications from U-Pb and Re-Os geochronology and Sr-Nd-Hf isotopes of the Luming Mo and Xulaojiugou Pb-Zn deposits. *J. Asian Earth Sci.* **2014**, *90*, 88–100. [[CrossRef](#)]
92. Liu, K.; Zhang, J.; Wilde, S.A.; Zhou, J.; Wang, M.; Ge, M.; Wang, J.; Ling, Y. Initial subduction of the Paleo-Pacific Oceanic plate in NE China: Constraints from whole-rock geochemistry and zircon U-Pb and Lu-Hf isotopes of the Khanka Lake granitoids. *Lithos* **2017**, *274*, 254–270. [[CrossRef](#)]
93. Long, X.Y.; Xu, W.L.; Guo, P.; Sun, C.Y.; Luan, J.P. Opening and closure history of the Mudanjiang Ocean in the eastern Central Asian Orogenic Belt: Geochronological and geochemical constraints from early Mesozoic intrusive rocks. *Gondwana Res.* **2020**, *84*, 111–130. [[CrossRef](#)]
94. Wu, F.Y.; Sun, D.Y.; Li, H.M.; Wang, X.L. The nature of basement beneath the Songliao Basin in NE China: Geochemical and isotopic constraints. *Phys. Chem. Earth Part A: Solid Earth Geod.* **2001**, *26*, 793–803. [[CrossRef](#)]
95. Wu, F.Y.; Walker, R.J.; Ren, X.W.; Sun, D.Y.; Zhou, X.H. Osmium isotopic constraints on the age of lithospheric mantle beneath northeastern China. *Chem. Geol.* **2003**, *196*, 107–129. [[CrossRef](#)]
96. Zhu, C.Y.; Zhao, G.; Ji, J.; Sun, M.; Han, Y.; Liu, Q.; Eizenhöfer, P.R.; Zhang, X.; Hou, W. Subduction between the Jiamusi and Songliao blocks: Geological, geochronological and geochemical constraints from the Heilongjiang Complex. *Lithos* **2017**, *282*, 128–144. [[CrossRef](#)]
97. Cheng, G.; Wang, R.; Zeng, Q.; Guo, Y.; Duan, X.; Wei, J.; Zhang, J.; Gao, X. Zircon U-Pb ages, Hf isotopes of the granitoids and Re-Os ages of the molybdenites in Luming molybdenum ore area, Heilongjiang Province, and its geological significance. *Acta Petrol. Sin.* **2015**, *31*, 2450–2464.
98. Sun, C.; Long, X.; Xu, W.; Wang, F.; Ge, W.; Guo, P.; Liu, X. Zircon U-Pb ages and Hf isotopic compositions of the Heilongjiang Complex from Jiayin, Heilongjiang Province and Kundur, Russian Far East and their geological implications. *Acta Petrol. Sin.* **2018**, *34*, 2901–2916.
99. Yang, Y.C.; Han, S.J.; Sun, D.Y.; Guo, J.; Zhang, S.J. Geological and geochemical features and geochronology of porphyry molybdenum deposits in the Lesser Xing'an Range-Zhangguangcai Range metallogenic belt. *Acta Petrol. Sin.* **2012**, *28*, 379–390.
100. Guo, P.; Xu, W.L.; Yu, J.J.; Wang, F.; Tang, J.; Li, Y. Geochronology and geochemistry of Late Triassic bimodal igneous rocks at the eastern margin of the Songnen-Zhangguangcai Range Massif, Northeast China: Petrogenesis and tectonic implications. *Int. Geol. Rev.* **2016**, *58*, 196–215. [[CrossRef](#)]
101. Han, W.; Zhou, J.B.; Wilde, S.A.; Li, L. LA-ICPMS zircon U-Pb dating of the Heilongjiang Complex in the Luobei area: New constraints for the late Palaeozoic-Mesozoic tectonic evolution of Jiamusi Block, NE China. *Geol. J.* **2020**, *55*, 1644–1669. [[CrossRef](#)]
102. Qin, J.F.; Lai, S.C.; Li, Y.F.; Ju, Y.J.; Zhu, R.Z.; Zhao, S.W. Early Jurassic monzogranite-tonalite association from the southern Zhangguangcai Range: Implications for paleo-Pacific plate subduction along northeastern China. *Lithosphere* **2016**, *8*, 396–411. [[CrossRef](#)]
103. Xu, W.L.; Ji, W.Q.; Pei, F.P.; Meng, E.; Yu, Y.; Yang, D.B.; Zhang, X. Triassic volcanism in eastern Heilongjiang and Jilin provinces, NE China: Chronology, geochemistry, and tectonic implications. *J. Asian Earth Sci.* **2009**, *34*, 392–402. [[CrossRef](#)]
104. Zhou, J.B.; Wilde, S.A.; Zhao, G.C.; Zhang, X.Z.; Zheng, C.Q.; Wang, H. New SHRIMP U-Pb zircon ages from the Heilongjiang high-pressure belt: Constraints on the Mesozoic evolution of NE China. *Am. J. Sci.* **2010**, *310*, 1024–1053. [[CrossRef](#)]

105. Guo, P.; Xu, W.L.; Wang, Z.W.; Wang, F.; Luan, J.P. Geochronology and geochemistry of Late Devonian-Carboniferous igneous rocks in the Songnen-Zhangguangcai Range Massif, NE China: Constraints on the late Paleozoic tectonic evolution of the eastern Central Asian Orogenic Belt. *Gondwana Res.* **2018**, *57*, 119–132. [[CrossRef](#)]
106. Wang, F.; Xu, W.L.; Gao, F.H.; Meng, E.; Cao, H.H.; Zhao, L.; Yang, Y. Tectonic history of the Zhangguangcailing Group in eastern Heilongjiang Province, NE China: Constraints from U-Pb geochronology of detrital and magmatic zircons. *Tectonophysics* **2012**, *566*, 105–122. [[CrossRef](#)]
107. Wang, F.; Xu, W.L.; Xu, Y.G.; Gao, F.H.; Ge, W.C. Late Triassic bimodal igneous rocks in eastern Heilongjiang Province, NE China: Implications for the initiation of subduction of the Paleo-Pacific Plate beneath Eurasia. *J. Asian Earth Sci.* **2015**, *97*, 406–423. [[CrossRef](#)]
108. Yang, H.; Ge, W.; Zhao, G.; Yu, J.; Zhang, Y. Early Permian-Late Triassic granitic magmatism in the Jiamusi-Khanka Massif, eastern segment of the Central Asian Orogenic Belt and its implications. *Gondwana Res.* **2015**, *27*, 1509–1533. [[CrossRef](#)]
109. Yang, H.; Ge, W.C.; Zhao, G.C.; Dong, Y.; Xu, W.L.; Ji, Z.; Yu, J.J. Late Triassic intrusive complex in the Jidong region, Jiamusi-Khanka Block, NE China: Geochemistry, zircon U-Pb ages, Lu-Hf isotopes, and implications for magma mingling and mixing. *Lithos* **2015**, *224*, 143–159. [[CrossRef](#)]
110. Zhou, J.B.; Wilde, S.A.; Zhang, X.Z.; Zhao, G.C.; Zheng, C.Q.; Wang, Y.J.; Zhang, X.H. The onset of Pacific margin accretion in NE China: Evidence from the Heilongjiang high-pressure metamorphic belt. *Tectonophysics* **2009**, *478*, 230–246. [[CrossRef](#)]
111. Zhou, J.B.; Wilde, S.A.; Zhao, G.C.; Zhang, X.Z.; Wang, H.; Zeng, W.S. Was the easternmost segment of the Central Asian Orogenic Belt derived from Gondwana or Siberia: An intriguing dilemma? *J. Geodyn.* **2010**, *50*, 300–317. [[CrossRef](#)]
112. Sun, D.Y.; Wu, F.Y.; Gao, S. LA-ICPMS zircon U-Pb age of the Qingshui pluton in the east Xiao Hinggan Mountains. *Acta Geosci. Sin.* **2004**, *25*, 213–218.
113. Cui, W.; Zeng, Z.; Zhang, X.; Liu, Z.; Wang, S.; Pu, J.; Fu, Q.; Guo, Y. Detrital Zircon U-Pb Dating of Nanshuangyashan Formation in the Jiamusi Massif, NE China and its Tectonic Implications. *Acta Geol. Sin.-Engl. Ed.* **2019**, *93*, 1559–1579. [[CrossRef](#)]
114. Meng, E.; Xu, W.L.; Pei, F.P.; Yang, D.B.; Yu, Y.; Zhang, X.Z. Detrital-zircon geochronology of Late Paleozoic sedimentary rocks in eastern Heilongjiang Province, NE China: Implications for the tectonic evolution of the eastern segment of the Central Asian Orogenic Belt. *Tectonophysics* **2010**, *485*, 42–51. [[CrossRef](#)]
115. Wang, F.; Xu, W.L.; Gao, F.H.; Zhang, H.H.; Pei, F.P.; Zhao, L.; Yang, Y. Precambrian terrane within the Songnen-Zhangguangcai Range Massif, NE China: Evidence from U-Pb ages of detrital zircons from the Dongfengshan and Tadong groups. *Gondwana Res.* **2014**, *26*, 402–413. [[CrossRef](#)]
116. Wang, Z.W.; Xu, W.L.; Pei, F.P.; Wang, F.; Guo, P. Geochronology and geochemistry of Early Paleozoic igneous rocks of the Lesser Xing'an Range, NE China: Implications for the tectonic evolution of the eastern Central Asian Orogenic Belt. *Lithos* **2016**, *261*, 144–163. [[CrossRef](#)]
117. Yang, H.; Ge, W.C.; Bi, J.H.; Wang, Z.H.; Tian, D.X.; Dong, Y.; Chen, H.J. The Neoproterozoic-early Paleozoic evolution of the Jiamusi Block, NE China and its East Gondwana connection: Geochemical and zircon U-Pb-Hf isotopic constraints from the Mashan Complex. *Gondwana Res.* **2018**, *54*, 102–121. [[CrossRef](#)]
118. Wilde, S.A.; Wu, F.Y.; Zhang, X.Z. The Mashan Complex: SHRIMP U-Pb zircon evidence for a Late Pan-African metamorphic event in NE China and its implication for global continental reconstructions. *Geochimica* **2001**, *30*, 35–50.
119. Dong, Y.; Ge, W.C.; Yang, H.; Xu, W.L.; Bi, J.H.; Wang, Z.H. Geochemistry and geochronology of the Late Permian mafic intrusions along the boundary area of Jiamusi and Songnen-Zhangguangcai Range massifs and adjacent regions, northeastern China: Petrogenesis and implications for the tectonic evolution of the Mudanjiang Ocean. *Tectonophysics* **2017**, *694*, 356–367.
120. Ge, M.H.; Zhang, J.J.; Liu, K.; Ling, Y.Y.; Wang, M.; Wang, J.M. Geochemistry and geochronology of the blueschist in the Heilongjiang Complex and its implications in the late Paleozoic tectonics of eastern NE China. *Lithos* **2016**, *261*, 232–249. [[CrossRef](#)]
121. Han, Z.Z.; Ren, X.; Schertl, H.P.; Li, X.P.; Song, Z.G.; Du, Q.X.; Chao, H.; Zhong, W.J.; Gao, L.H. Zircon U-Pb-Hf isotopes and geochemistry of Jurassic igneous rocks from the southern Zhangguangcai Range, NE China: Constraints on magmatism, petrogenesis and tectonic implications. *Int. Geol. Rev.* **2020**, *62*, 1988–2012. [[CrossRef](#)]
122. Li, W.; Takasu, A.; Liu, Y.; Genser, J.; Zhao, Y.; Han, G.; Guo, X. U-Pb and  $^{40}\text{Ar}/^{39}\text{Ar}$  age constrains on protolith and high-P/T type metamorphism of the Heilongjiang Complex in the Jiamusi Massif, NE China. *J. Mineral. Petrol. Sci.* **2011**, *106*, 326–331. [[CrossRef](#)]
123. Long, X.Y.; Xu, W.L.; Guo, P.; Sun, C.Y.; Luan, J.P. Was Permian magmatism in the eastern Songnen and western Jiamusi massifs, NE China, related to the subduction of the Mudanjiang oceanic plate? *Geol. J.* **2020**, *55*, 1781–1807. [[CrossRef](#)]
124. Wu, F.Y.; Yang, J.H.; Lo, C.H.; Wilde, S.A.; Sun, D.Y.; Jahn, B.M. The Heilongjiang Group: A Jurassic accretionary complex in the Jiamusi Massif at the western Pacific margin of northeastern China. *Isl. Arc.* **2007**, *16*, 156–172. [[CrossRef](#)]
125. Xing, K.C.; Wang, F.; Xu, W.L.; Gao, F.H. Tectonic affinity of the Khanka Massif in the easternmost Central Asian Orogenic Belt: Evidence from detrital zircon geochronology of Permian sedimentary rocks. *Int. Geol. Rev.* **2020**, *62*, 428–445. [[CrossRef](#)]
126. Yang, H.; Ge, W.; Dong, Y.; Bi, J.; Wang, Z.; Ji, Z. Record of Permian-Early Triassic continental arc magmatism in the western margin of the Jiamusi Block, NE China: Petrogenesis and implications for Paleo-Pacific subduction. *Int. J. Earth Sci.* **2017**, *106*, 1919–1942. [[CrossRef](#)]

127. Yang, H.; Ge, W.C.; Dong, Y.; Bi, J.H.; Ji, Z.; He, Y.; Jing, Y.; Xu, W.L. Permian subduction of the Paleo-Pacific (Panthalassic) oceanic lithosphere beneath the Jiamusi Block: Geochronological and geochemical evidence from the Luobei mafic intrusions in Northeast China. *Lithos* **2019**, *332*, 207–225. [[CrossRef](#)]
128. Yu, J.; Wang, F.; Xu, W.; Gao, F.; Tang, J. Late Permian tectonic evolution at the southeastern margin of the Songnen-Zhangguangcai Range Massif, NE China: Constraints from geochronology and geochemistry of granitoids. *Gondwana Res.* **2013**, *24*, 635–647. [[CrossRef](#)]
129. Zhu, C.Y.; Zhao, G.; Sun, M.; Eizenhöfer, P.R.; Liu, Q.; Zhang, X.; Han, Y.; Hou, W. Geochronology and geochemistry of the Yilan greenschists and amphibolites in the Heilongjiang complex, northeastern China and tectonic implications. *Gondwana Res.* **2017**, *43*, 213–228. [[CrossRef](#)]
130. Bi, J.H.; Ge, W.C.; Yang, H.; Wang, Z.H.; Dong, Y.; Liu, X.W.; Ji, Z. Age, petrogenesis, and tectonic setting of the Permian bimodal volcanic rocks in the eastern Jiamusi Massif, NE China. *J. Asian Earth Sci.* **2017**, *134*, 160–175. [[CrossRef](#)]
131. Bi, J.H.; Ge, W.C.; Yang, H.; Wang, Z.H.; Xu, W.L.; Yang, J.H.; Xing, D.H.; Chen, H.J. Geochronology and geochemistry of late Carboniferous-middle Permian I-and A-type granites and gabbro-diorites in the eastern Jiamusi Massif, NE China: Implications for petrogenesis and tectonic setting. *Lithos* **2016**, *266*, 213–232. [[CrossRef](#)]
132. Bi, J.H.; Ge, W.C.; Yang, H.; Zhao, G.C.; Xu, W.L.; Wang, Z.H. Geochronology, geochemistry and zircon Hf isotopes of the Dongfanghong gabbroic complex at the eastern margin of the Jiamusi Massif, NE China: Petrogenesis and tectonic implications. *Lithos* **2015**, *234*, 27–46. [[CrossRef](#)]
133. Chen, Z.; Liu, Y.; Guan, Q. Convergence history of the Songliao and Jiamusi blocks in the eastern end of Central Asian Orogenic Belt: Evidence from detrital zircons of Late Paleozoic sedimentary rocks. *Acta Geol. Sin.-Engl. Ed.* **2019**, *93*, 1417–1433. [[CrossRef](#)]
134. Dong, Y.; Ge, W.; Yang, H.; Bi, J.; Wang, Z.; Xu, W. Permian tectonic evolution of the Mudanjiang Ocean: Evidence from zircon U-Pb-Hf isotopes and geochemistry of a NS trending granitoid belt in the Jiamusi Massif, NE China. *Gondwana Res.* **2017**, *49*, 147–163. [[CrossRef](#)]
135. Dong, Y.; Ge, W.C.; Yang, H.; Liu, X.W.; Bi, J.H.; Ji, Z.; Xu, W.L. Geochemical and SIMS U-Pb rutile and LA-ICP-MS U-Pb zircon geochronological evidence of the tectonic evolution of the Mudanjiang Ocean from amphibolites of the Heilongjiang Complex, NE China. *Gondwana Res.* **2019**, *69*, 25–44. [[CrossRef](#)]
136. Dong, Y.; He, Z.H.; Ren, Z.H.; Ge, W.C.; Yang, H.; Ji, Z.; He, Y. Formation of the Permian Taipinggou igneous rocks, north of Luobei (Northeast China): Implications for the subduction of the Mudanjiang Ocean beneath the Bureya-Jiamusi Massif. *Int. Geol. Rev.* **2018**, *60*, 1195–1212. [[CrossRef](#)]
137. Meng, E.; Xu, W.L.; Pei, F.P.; Yang, D.B.; Wang, F.; Zhang, X.Z. Permian bimodal volcanism in the Zhangguangcai Range of eastern Heilongjiang Province, NE China: Zircon U-Pb-Hf isotopes and geochemical evidence. *J. Asian Earth Sci.* **2011**, *41*, 119–132. [[CrossRef](#)]
138. Sun, M.D.; Xu, Y.G.; Wilde, S.A.; Chen, H.L.; Yang, S.F. The Permian Dongfanghong island-arc gabbro of the Wandashan Orogen, NE China: Implications for Paleo-Pacific subduction. *Tectonophysics* **2015**, *659*, 122–136. [[CrossRef](#)]
139. Dong, C. Tectonic Evolution of the Jiamusi Massif: Constrains from Late Paleozoic Sedimentary-Volcanic Rocks. Ph.D. Thesis, Jilin University, Changchun, China, 2013.
140. Meng, E.; Xu, W.L.; Pei, F.P.; Wang, F. Middle Devonian volcanism in eastern Heilongjiang Province and its tectonic implications: Constraints from petro-geochemistry, zircon U-Pb chronology and Sr-Nd-Hf isotopes. *Acta Petrol. Et Mineral.* **2011**, *30*, 883–900.
141. Bi, J.H.; Ge, W.C.; Yang, H.; Zhao, G.C.; Yu, J.J.; Zhang, Y.L.; Wang, Z.H.; Tian, D.X. Petrogenesis and tectonic implications of early Paleozoic granitic magmatism in the Jiamusi Massif, NE China: Geochronological, geochemical and Hf isotopic evidence. *J. Asian Earth Sci.* **2014**, *96*, 308–331. [[CrossRef](#)]
142. Wilde, S.A.; Wu, F.Y.; Zhao, G. The Khanka Block, NE China, and its significance for the evolution of the Central Asian Orogenic Belt and continental accretion. *Geol. Soc. Lond. Spec. Publ.* **2010**, *338*, 117–137. [[CrossRef](#)]
143. Yang, H.; Ge, W.C.; Zhao, G.C.; Bi, J.H.; Wang, Z.H.; Dong, Y.; Xu, W.L. Zircon U-Pb ages and geochemistry of newly discovered Neoproterozoic orthogneisses in the Mishan region, NE China: Constraints on the high-grade metamorphism and tectonic affinity of the Jiamusi-Khanka Block. *Lithos* **2017**, *268*, 16–31. [[CrossRef](#)]
144. Yang, H.; Ge, W.C.; Zhao, G.C.; Dong, Y.; Bi, J.H.; Wang, Z.H.; Yu, J.J.; Zhang, Y.L. Geochronology and geochemistry of Late Pan-African intrusive rocks in the Jiamusi-Khanka Block, NE China: Petrogenesis and geodynamic implications. *Lithos* **2014**, *208*, 220–236. [[CrossRef](#)]
145. Song, B.; Li, J.Y.; Niu, B.G.; Xu, W.X. Single-grain zircon ages and its implications in biotite-plagioclase gneiss in Mashan Group in the eastern Heilongjiang. *Acta Geosci. Sin.* **1997**, *18*, 306–312.
146. Alenicheva, A.A.; Sakhno, V.G.; Saltykova, T.E. U-Pb and Rb-Sr dating of granitoids from the Tatibin Group in the plutonic belt of Central Sikhote Alin. *In Dokl. Earth Sci.* **2008**, *420*, 533–537. [[CrossRef](#)]
147. Jahn, B.M.; Valui, G.; Kruk, N.; Gonevchuk, V.; Usuki, M.; Wu, J.T. Emplacement ages, geochemical and Sr-Nd-Hf isotopic characterization of Mesozoic to early Cenozoic granitoids of the Sikhote-Alin Orogenic Belt, Russian Far East: Crustal growth and regional tectonic evolution. *J. Asian Earth Sci.* **2015**, *111*, 872–918. [[CrossRef](#)]
148. Tang, J.; Xu, W.; Niu, Y.; Wang, F.; Ge, W.; Sorokin, A.A.; Chekryzhov, I.Y. Geochronology and geochemistry of Late Cretaceous-Paleocene granitoids in the Sikhote-Alin Orogenic Belt: Petrogenesis and implications for the oblique subduction of the paleo-Pacific plate. *Lithos* **2016**, *266*, 202–212. [[CrossRef](#)]

149. Zhao, P.; Jahn, B.M.; Xu, B. Elemental and Sr-Nd isotopic geochemistry of Cretaceous to Early Paleogene granites and volcanic rocks in the Sikhote-Alin Orogenic Belt (Russian Far East): Implications for the regional tectonic evolution. *J. Asian Earth Sci.* **2017**, *146*, 383–401. [[CrossRef](#)]
150. Wang, Z.H.; Ge, W.C.; Yang, H.; Zhang, Y.L.; Bi, J.H.; Tian, D.X.; Xu, W.L. Middle Jurassic oceanic island igneous rocks of the Raohe accretionary complex, northeastern China: Petrogenesis and tectonic implications. *J. Asian Earth Sci.* **2015**, *111*, 120–137. [[CrossRef](#)]
151. Zhang, D.; Liu, Y.J.; Li, W.M.; Li, S.Z.; Iqbal, M.Z.; Chen, Z.X. Marginal accretion processes of Jiamusi Block in NE China: Evidences from detrital zircon U-Pb age and deformation of the Wandashan Terrane. *Gondwana Res.* **2020**, *78*, 92–109. [[CrossRef](#)]
152. Zhou, J.B.; Cao, J.L.; Wilde, S.A.; Zhao, G.C.; Zhang, J.J.; Wang, B. Paleo-Pacific subduction-accretion: Evidence from geochemical and U-Pb zircon dating of the Nadanhada accretionary complex, NE China. *Tectonics* **2014**, *33*, 2444–2466. [[CrossRef](#)]
153. Cheng, R.Y.; Wu, F.Y.; Ge, W.C.; Sun, D.Y.; Liu, X.M.; Yang, J.H. Emplacement age of the Raohe Complex in eastern Heilongjiang Province and the tectonic evolution of the eastern part of Northeastern China. *Acta Petrol. Sin.* **2006**, *22*, 353–376.
154. Liu, K.; Zhang, J.; Wilde, S.A.; Liu, S.; Guo, F.; Kasatkin, S.A.; Golozoubov, V.V.; Ge, M.; Wang, M.; Wang, J. U-Pb dating and Lu-Hf isotopes of detrital zircons from the southern Sikhote-Alin orogenic belt, Russian Far East: Tectonic implications for the Early Cretaceous evolution of the Northwest Pacific margin. *Tectonics* **2017**, *36*, 2555–2598. [[CrossRef](#)]
155. Sun, M.D.; Xu, Y.G.; Wilde, S.A.; Chen, H.L. Provenance of Cretaceous trench slope sediments from the Mesozoic Wandashan Orogen, NE China: Implications for determining ancient drainage systems and tectonics of the Paleo-Pacific. *Tectonics* **2015**, *34*, 1269–1289. [[CrossRef](#)]
156. Wang, F.; Xu, W.L.; Xing, K.C.; Tang, J.; Wang, Z.W.; Sun, C.Y.; Wu, W. Temporal changes in the subduction of the Paleo-Pacific plate beneath Eurasia during the Late Mesozoic: Geochronological and geochemical evidence from Cretaceous volcanic rocks in eastern NE China. *Lithos* **2019**, *326*, 415–434. [[CrossRef](#)]
157. He, S. Geochronological, geochemical characteristics and tectonic setting of granitic rocks in the Hulin area Heilongjiang Province. Master's Thesis, Jilin University, Changchun, China, 2017.
158. Liu, C.; Zhu, G.; Zhang, S.; Gu, C.; Li, Y.; Su, N.; Xiao, S. Mesozoic strike-slip movement of the Dunhua-Mishan Fault Zone in NE China: A response to oceanic plate subduction. *Tectonophysics* **2018**, *723*, 201–222. [[CrossRef](#)]
159. Ling, Y.Y.; Zhang, J.J.; Liu, K.; Ge, M.H.; Wang, M.; Wang, J.M. Geochemistry, geochronology, and tectonic setting of Early Cretaceous volcanic rocks in the northern segment of the Tan-Lu Fault region, northeast China. *J. Asian Earth Sci.* **2017**, *144*, 303–322. [[CrossRef](#)]
160. Wen, Q.B.; Liu, Y.J.; Liu, B.; Han, G.Q.; Zhao, Y.L.; Li, W.; Liang, C.Y. Exhumation time of Jiamusi-uplift of northeastern China constrained by ages of detrital minerals. *Geol. Bull. China* **2011**, *30*, 250–257.
161. Anders, M.H.; Spiegelman, M.; Rodgers, D.W.; Hagstrum, J.T. The growth of fault-bounded tilt blocks. *Tectonics* **1993**, *12*, 1451–1459. [[CrossRef](#)]
162. Howard, K.A.; Beard, L.S.; Kuntz, M.A.; Kunk, M.J.; Sarna-Wojcicki, A.M.; Perkins, M.E.; Lucchitta, I. Erosion of tilted fault blocks and deposition of coarse sediments in half-graben basins during late stages of extension: Gold Butte area, Basin and Range Province. *Miocene Tecton. Lake Mead Reg. Cent. Basin Range Geol. Soc. Am. Spec. Pap.* **2010**, *463*, 147–170.
163. Gawthorpe, R.L.; Leeder, M.R. Tectono-sedimentary evolution of active extensional basins. *Basin Res.* **2000**, *12*, 195–218. [[CrossRef](#)]
164. Zhao, X.; Chen, H.; Zhang, F.; Sun, M.; Yang, J.; Tan, B. Characteristics, structural styles and tectonic implications of Mesozoic-Cenozoic faults in the eastern Heilongjiang basins (NE China). *J. Asian Earth Sci.* **2017**, *146*, 196–210. [[CrossRef](#)]
165. Wang, T.; Guo, L.; Zhang, L.; Yang, Q.; Zhang, J.; Tong, Y.; Ye, K. Timing and evolution of Jurassic-Cretaceous granitoid magmatism in the Mongol-Okhotsk belt and adjacent areas, NE Asia: Implications for transition from contractional crustal thickening to extensional thinning and geodynamic settings. *J. Asian Earth Sci.* **2015**, *97*, 365–392. [[CrossRef](#)]
166. Li, K.; Jolivet, M.; Zhang, Z.; Li, J.; Tang, W. Long-term exhumation history of the Inner Mongolian Plateau constrained by apatite fission track analysis. *Tectonophysics* **2016**, *666*, 121–133. [[CrossRef](#)]
167. Yang, Y.T. An unrecognized major collision of the Okhotomorsk Block with East Asia during the Late Cretaceous, constraints on the plate reorganization of the Northwest Pacific. *Earth-Sci. Rev.* **2013**, *126*, 96–115. [[CrossRef](#)]
168. Li, S.; Suo, Y.; Li, X.; Zhou, J.; Santosh, M.; Wang, P.; Wang, G.; Guo, L.; Tu, S.; Lan, H.; et al. Mesozoic tectono-magmatic response in the East Asian ocean-continent connection zone to subduction of the Paleo-Pacific Plate. *Earth-Sci. Rev.* **2019**, *192*, 91–137. [[CrossRef](#)]
169. Zhang, K.J.; Yan, L.L.; Ji, C. Switch of NE Asia from extension to contraction at the mid-Cretaceous: A tale of the Okhotsk oceanic plateau from initiation by the Perm Anomaly to extrusion in the Mongol-Okhotsk ocean? *Earth-Sci. Rev.* **2019**, *198*, 102941. [[CrossRef](#)]
170. Ryu, I.C.; Lee, C. Intracontinental mantle plume and its implications for the Cretaceous tectonic history of East Asia. *Earth Planet. Sci. Lett.* **2017**, *479*, 206–218. [[CrossRef](#)]
171. Huang, Q.H.; Wu, H.C.; Wan, X.Q.; He, H.Y.; Deng, C.L. New progress of integrated chronostratigraphy of the Cretaceous in Songliao Basin. *J. Stratigr.* **2011**, *35*, 250–257.
172. Pei, F.P.; Xu, W.L.; Yang, D.B.; Ji, W.Q.; Yu, Y.; Zhang, X.Z. Mesozoic volcanic rocks in the southern Songliao Basin: Zircon U-Pb ages and their constraints on the nature of basin basement. *Earth Sci. J. China Univ. Geosci.* **2008**, *5*, 603–617.
173. Wang, C.L.; Zhang, M.S.; Sun, K.; Wang, Y.; Li, X.; Liu, X. Latest zircon U-Pb geochronology of the huoshiling formation volcanic rocks in the southeastern margin of the Songliao Basin. *Acta Geol. Sin. Engl. Ed.* **2017**, *91*, 1924–1925. [[CrossRef](#)]

174. Yu, Z.Q.; He, H.Y.; Deng, C.L.; Lu, K.; Shen, Z.; Li, Q. New SIMS U-Pb geochronology for the shahezi formation from CCSD-SK-IIe borehole in the Songliao Basin, NE China. *Sci. Bull.* **2020**, *65*, 1049–1051. [[CrossRef](#)]
175. Liu, H.; Wang, P.; Gao, Y.; Yin, Y.; Li, H. New data from ICDP borehole SK2 and its constraint on the beginning of the Lower Cretaceous Shahezi Formation in the Songliao Basin, NE China. *Sci. Bull.* **2021**, *66*, 411–413. [[CrossRef](#)]
176. Liu, W.; Wu, H.; Hinnov, L.A.; Baddouh, M.B.; Wang, P.; Gao, Y.; Zhang, S.; Yang, T.; Li, Y.; Wang, C. An 11 million-year-long record of astronomically forced fluvial-alluvial deposition and paleoclimate change in the Early Cretaceous Songliao synrift basin, China. *Palaeogeogr. Palaeoclimatol. Palaeoecol.* **2020**, *541*, 109555. [[CrossRef](#)]
177. Wang, T.; Wang, C.; Ramezani, J.; Wan, X.; Yu, Z.; Gao, Y.; He, H.; Wu, H. High-precision geochronology of the Early Cretaceous Yingcheng Formation and its stratigraphic implications for Songliao Basin, China. *Geosci. Front.* **2022**, *13*, 101386. [[CrossRef](#)]
178. Guo, Z.X.; Shi, Y.P.; Yang, Y.T.; Jiang, S.Q.; Li, L.B.; Zhao, Z.G. Inversion of the Erlian Basin (NE China) in the early Late Cretaceous: Implications for the collision of the Okhotomorsk Block with East Asia. *J. Asian Earth Sci.* **2018**, *154*, 49–66. [[CrossRef](#)]
179. Zhang, Y.Q.; Zhao, Y.; Dong, S.W. Tectonic evolution stages of the Early Cretaceous rift basins in Eastern China and adjacent areas and their geodynamic background. *Earth Sci. Front.* **2004**, *11*, 123–134.
180. Li, J.; Zhang, Y.; Dong, S.; Johnston, S.T. Cretaceous tectonic evolution of South China: A preliminary synthesis. *Earth-Sci. Rev.* **2014**, *134*, 98–136. [[CrossRef](#)]
181. Song, Y.; Stepashko, A.A.; Ren, J. The Cretaceous climax of compression in Eastern Asia: Age 87–89 Ma (late Turonian/Coniacian), Pacific cause, continental consequences. *Cretac. Res.* **2015**, *55*, 262–284. [[CrossRef](#)]
182. Mercier, J.L.; Vergely, P.; Zhang, Y.Q.; Hou, M.J.; Bellier, O.; Wang, Y.M. Structural records of the late Cretaceous-Cenozoic extension in Eastern China and the kinematics of the Southern Tan-Lu and Qinling fault zone (Anhui and Shaanxi provinces, PR China). *Tectonophysics* **2013**, *582*, 50–75. [[CrossRef](#)]
183. Chen, Y.; Meng, J.; Liu, H.; Wang, C.; Tang, M.; Liu, T.; Zhao, Y. Detrital zircons record the evolution of the Cathaysian Coastal Mountains along the South China margin. *Basin Res.* **2022**, *34*, 688–701. [[CrossRef](#)]
184. Suo, Y.; Li, S.; Cao, X.; Wang, X.; Somerville, I.; Wang, G.; Wang, P.; Liu, B. Mesozoic-Cenozoic basin inversion and geodynamics in East China: A review. *Earth-Sci. Rev.* **2020**, *210*, 103357. [[CrossRef](#)]
185. Tan, J.; Zhang, L.; Wang, C.; Cao, K.; Li, X. Late Cretaceous provenance change in the Jiaolai Basin, East China: Implications for paleogeographic evolution of East Asia. *J. Asian Earth Sci.* **2020**, *194*, 104188. [[CrossRef](#)]
186. Yu, X.; Liu, C.; Wang, C.; Wang, J. Late Cretaceous aeolian desert system within the Mesozoic fold belt of South China: Palaeoclimatic changes and tectonic forcing of East Asian erg development and preservation. *Palaeogeogr. Palaeoclimatol. Palaeoecol.* **2021**, *567*, 110299. [[CrossRef](#)]
187. Zhang, L.; Zhang, C.; Dou, L. Palaeoenvironment Implication of Red Paleosols in a Late Cretaceous Continental Succession, Songliao Basin, NE China. *Minerals* **2021**, *11*, 993. [[CrossRef](#)]
188. Li, J.; Shu, L. Mesozoic-Cenozoic tectonic features and evolution of the Song-Liao Basin, NE China. *J.-Nanjing Univ. Nat. Sci. Ed.* **2002**, *38*, 525–531.
189. Cao, C.Y.; Dong, X.W. Tectonics and deep structure features of Meso-Cenozoic basin groups, northern NE China. *Coal Geol. Explor.* **2008**, *36*, 1–5.
190. Chengzhi, Y. Comparative Study on Late Cretaceous Tectonic Inversion of Songliao Basin-Great Sanjiang Basin and its Genetic Relationships. Ph.D. Thesis, China University of Geosciences, Wuhan, China, 2014.
191. Zhu, G.; Liu, C.; Gu, C.; Zhang, S.; Li, Y.; Su, N.; Xiao, S. Oceanic plate subduction history in the western Pacific Ocean: Constraint from late Mesozoic evolution of the Tan-Lu Fault Zone. *Sci. China Earth Sci.* **2018**, *61*, 386–405. [[CrossRef](#)]
192. Zhu, G.; Niu, M.; Xie, C.; Wang, Y. Sinistral to normal faulting along the Tan-Lu fault zone: Evidence for geodynamic switching of the East China continental margin. *J. Geol.* **2010**, *118*, 277–293. [[CrossRef](#)]
193. Kirillova, G.L. Cretaceous tectonic and biotic evolution of the southeastern Russian continental margin. *Isl. Arc.* **2018**, *27*, e12238. [[CrossRef](#)]
194. Kim, J.S.; Cho, H.; Son, M.; Sohn, Y.K. Geological age of the Gyeongsang Supergroup. In Proceedings of the Fall Joint Annual Conference of The Geological Societies in Korea (Abstract), Jeju, Korea, 26–29 October 2011; Volume 2.
195. Kim, Y.B.; Chwae, U.; Hwang, S.K. *Geological Report of the Changamjeon Sheet, (1: 50000)*; Korea Institute of Geoscience and Mineral Resources: Daejeon, Korea, 2010.
196. Ko, K.; Kim, S.; Gihm, Y. U-Pb Age Dating and Geochemistry of Soft-Sediment Deformation Structure-Bearing Late Cretaceous Volcano-Sedimentary Basins in the SW Korean Peninsula and Their Tectonic Implications. *Minerals* **2021**, *11*, 520. [[CrossRef](#)]
197. Ko, K.; Kim, S.W.; Lee, H.J.; Hwang, I.G.; Kim, B.C.; Kee, W.S.; Kim, Y.S.; Gihm, Y.S. Soft sediment deformation structures in a lacustrine sedimentary succession induced by volcano-tectonic activities: An example from the Cretaceous Beolgeumri Formation, Wido Volcanics, Korea. *Sediment. Geol.* **2017**, *358*, 197–209. [[CrossRef](#)]
198. Kwon, C.W.; Ko, K.; Gihm, Y.S.; Koh, H.J.; Kim, H. Late Cretaceous volcanic arc system in southwest Korea: Distribution, lithology, age, and tectonic implications. *Cretac. Res.* **2017**, *75*, 125–140. [[CrossRef](#)]
199. Lee, Y.; Cheon, Y.; Ha, S.; Kang, H.C.; Son, M. Distribution, age, and structural evolution of the Goseong Formation in the southern Gyeongsang basin, SE Korea. *Journal of the Geological Society of Korea. J. Geol. Soc. Korea* **2018**, *54*, 359–381. [[CrossRef](#)]
200. Lee, S.H.; Oh, C.W.; Park, J.W. The age and geochemistry of the mid-Cretaceous volcanic rocks in the Jinan Basin: Implications for the mid-Cretaceous tectonic environments of the Korean Peninsula and Northeast Asia. *Lithos* **2020**, *358*, 105383. [[CrossRef](#)]

- 
201. Cheon, Y.; Ha, S.; Lee, S.; Son, M. Tectonic evolution of the Cretaceous Gyeongsang Back-arc Basin, SE Korea: Transition from sinistral transtension to strike-slip kinematics. *Gondwana Res.* **2020**, *83*, 16–35. [[CrossRef](#)]
  202. Chough, S.K.; Sohn, Y.K. Tectonic and sedimentary evolution of a Cretaceous continental arc-backarc system in the Korean peninsula: New view. *Earth-Sci. Rev.* **2010**, *101*, 225–249. [[CrossRef](#)]